Energy dissipation in the inner surf zone: new insights from LiDAR-based roller geometry measurements

K. Martins[1,2], **C. E. Blenkinsopp**[1], **R. Deigaard**[3], **H. E. Power**[4]

[1]Research Unit for Water, Environment and Infrastructure Resilience (WEIR), University of Bath, UK.
[2]UMR 7266 LIENSs, CNRS - Université de La Rochelle, France
[3]DHI, Agern Allé 5, DK-2970 Hørsholm Denmark
[4]University of Newcastle, Australia

Key Points:

- Surface roller length and angle are extracted from an innovative LiDAR field dataset of broken waves propagating in the inner surf zone
- The influence of the roller area formulation on the parameterization of energy dissipation from *Duncan* [1981] is investigated
- Based on deep water wave breaking results, a new scaling law for energy dissipation in the inner surf zone is proposed

Corresponding author: K. Martins, k.martins@bath.ac.uk, kevin.martins@univ-lr.fr

Abstract

The spatial and temporal variation of energy dissipation rates in breaking waves controls the mean circulation of the surf zone. As this circulation plays an important role in the morphodynamics of beaches, it is vital to develop better understanding of the energy dissipation processes in breaking and broken waves. In this paper we present the first direct field measurements of roller geometry extracted from a LiDAR dataset of broken waves to obtain new insights into wave energy dissipation in the inner surf zone. We use a roller model to show that most existing roller area formulations in the literature lead to considerable overestimation of the wave energy dissipation, which is found to be close to, but smaller than, the energy dissipation in a hydraulic jump of the same height. The role of the roller density is also investigated, and we propose that it should be incorporated into modified roller area formulations until better knowledge of the roller area and its link with the mean roller density is acquired. Finally, using previously published results from deep-water wave breaking studies, we propose a scaling law for energy dissipation in the inner surf zone, which achieves satisfactory results at both the time-averaged and wave-by-wave scales.

1 Introduction

The surf zone is the part of the nearshore characterized by breaking and broken waves, which extends from the break point of the largest waves to the shoreline. Although the process of breaking can stop as waves propagate in deeper water (e.g. for bar/trough systems), two regions are generally used to describe the wave transformation after the break point: the outer surf zone, where the breaking wave exhibits rapid transformation just after breaking, and the inner surf zone, where the changes in shape are more gradual [*Svendsen et al.*, 1978; *Basco*, 1985]. In the outer surf zone, a considerable amount of incident wave energy is transformed through the entrainment of air, the generation of turbulent kinetic energy and vortices, splashes, noise and through sediment transport [e.g., *Peregrine*, 1983; *Battjes*, 1988; *Rapp and Melville*, 1990; *Deane*, 1997; *Blenkinsopp and Chaplin*, 2007; *Iafrati*, 2011]. In the inner surf zone, the primary processes leading to dissipation are the generation of turbulent kinetic energy and bed friction [*Peregrine*, 1983; *Svendsen*, 1984; *Stive and Wind*, 1986; *Deigaard et al.*, 1991]. As the energy dissipation and its spatial variation drive the mean circulation of the surf zone (undertow, alongshore currents but also macro vortices, e.g., see *Peregrine and Bokhove*, 1998; *Bühler and Jacobson*, 2001; *Brocchini et al.*, 2004; *Bonneton et al.*, 2010), acquiring a better understanding of energy dissipation rates due to wave breaking in the surf zone is valuable and required for modelling purposes.

Over the last few decades, numerical models based on the full Navier-Stokes equations have been increasingly used to study wave breaking processes [e.g., see *Lin and Liu*, 1998; *Jacobsen et al.*, 2012; *Higuera et al.*, 2013; *Deike et al.*, 2016]. However, they remain a limited tool for many engineering applications as they have high computational cost and it is often difficult to obtain the correct boundary conditions for the domain being modelled. Other phase-resolving models include those based on Boussinesq-type equations [e.g., see *Madsen and Schäffer*, 1998; *Lannes and Bonneton*, 2009] and the non-linear shallow water equations [NLSWE; e.g., *Raubenheimer*, 2002; *Bonneton*, 2007; *Zijlema and Stelling*, 2008]. These models accurately describe wave transformation up to the break point (refraction, diffraction, shoaling) with a much lower computational cost. However, they are incapable of describing the physics of wave overturning or water/air phase mixing and thus require special treatment for incorporating wave breaking-related processes [*Brocchini*, 2013]. For instance, the breaking onset and cessation need to be imposed in Boussinesq-type models, meaning that a parameterization for the energy dissipation due to wave breaking is also needed. Three principal approaches have been used in the literature for this: 1) the use of the roller concept [*Brocchini et al.*, 1992; *Schäffer et al.*, 1993; *Cienfuegos et al.*, 2010]; 2) an eddy-viscosity approach [*Zelt*, 1991; *Kennedy et al.*, 2000;

Klonaris et al., 2016]; and 3) the use of a shock-capturing NLSWE solver after the break point [*Tissier et al.*, 2012].

Introduced by *Svendsen et al.* [1978], the roller concept for depth-induced wave breaking accounts for the turbulent mass of mixed air and water advected by the breaker and the extra surface stresses that it generates, which affect the mean circulation [*Longuet-Higgins and Stewart*, 1964; *Svendsen et al.*, 1978; *Svendsen*, 1984; *Stive and Wind*, 1986; *Deigaard and Fredsøe*, 1989; *Nairn et al.*, 1990; *Deigaard*, 1993; *Rattanapitikon and Shibayama*, 2000; *Bae et al.*, 2013]. Unlike the eddy-viscosity approach mentioned above, the roller concept has the particular advantage that it provides both phase-resolving or phase-averaged models with a physical framework for parameterizing wave breaking processes in the surf zone. *Svendsen* [1984, hereafter S84] used the dissipation rate of a hydraulic jump of equivalent height, following the seminal work of *Le Méhauté* [1962]; *Hwang and Divoky* [1970]; *Battjes and Janssen* [1978]. The original approach of *Battjes and Janssen* [1978] is a common method to parameterize the energy dissipation rates due to wave breaking in shallow water in fully spectral models [e.g., *Benoit et al.*, 1996; *Vink*, 2001; *Cavaleri et al.*, 2007; *Salmon et al.*, 2015] and in simpler energy balance-based models [e.g., *Thornton and Guza*, 1983; *Stive*, 1984; *Svendsen*, 1984; *Battjes and Stive*, 1985; *Baldock et al.*, 1998]. It is important to note that in the studies cited above, the roller is not directly involved in the energy dissipation processes but serves only to better predict wave setup and mean cross-shore or alongshore currents.

An approach to parameterize energy dissipation rates in breaking waves directly from surface roller properties is possible based on the empirical relations observed by *Duncan* [1981, hereafter D81] for steady breakers generated by a hydrofoil. By varying the hydrofoil speed and angle of attack, D81 could relate the momentum deficit in the mean flow to the shearing forces exerted by the breaking region on the forward wave slope. The energy dissipation hence occurs at the roller/wave interface through shear stresses, which over the whole interface $L_r/\cos\theta$, can be expressed as:

$$\tau = \rho_r g A \sin\theta \tag{1}$$

where ρ_r is the mean water density over the roller area region A, g is the gravity constant, θ is the roller angle, and L_r is the roller length, see Figure 1 and Table 1 for a list of the parameters used in this study. Note that in this study, roller length is defined as the horizontal distance between the roller crest and toe, following *Haller and Catalán* [2009]. Hence, L_r is related to the total roller length L of D81 by $L = L_r/\cos\theta$. Eq. 1 has been used in many studies to model or estimate the energy dissipation due to wave breaking [*Dally and Brown*, 1995; *Lippmann et al.*, 1996; *Walstra et al.*, 1996; *Reniers and Battjes*, 1997; *Ruessink et al.*, 2001; *Haller and Catalán*, 2009; *Carini et al.*, 2015; *Flores et al.*, 2016]. However, very few studies report measurements of roller properties, whether external (θ, L_r) or internal (ρ_r, A). Roller lengths L_r have been estimated from video imagery in the study of *Haller and Catalán* [2009], and more recently by *Carini et al.* [2015] and *Flores et al.* [2016]. *Haller and Catalán* [2009] obtained a good match between remotely-sensed roller lengths and those inferred from their roller model. To estimate wave slopes in the dataset of *Haller and Catalán* [2009], *Zhang et al.* [2014] used the time elapsed between the upcrossing of the Mean Water Level (MWL) and the crest level, assuming a constant celerity from solitary wave theory. A similar method was used by *Carini et al.* [2015] but using the trough level and the celerity from linear wave theory. These estimates are valuable but can be considered quite coarse given that average wave celerity has been shown to be on average 1.14 times that given by linear wave theory in the surf zone [*Tissier et al.*, 2011], and that the preceding trough can be located well away from the bore toe (e.g. Figure 1 and 3 of D81). Nonetheless, *Zhang et al.* [2014] reported broken wave slopes greater than 0.2, which is at least twice the value of 0.1 generally adopted for $\tan\theta$ in energy balance-based models using the roller concept [e.g., *Dally and Brown*, 1995; *Walstra et al.*, 1996; *Reniers and Battjes*, 1997; *Ruessink et al.*, 2001; *Flores et al.*, 2016].

Considerable uncertainties also exist in our knowledge of the surface roller area A and mean density ρ_r. The quantity A represents the area of the surface roller located in front of the breaker above the oscillatory wave motion and characterized by turbulent and aerated flows [*Basco*, 1985]. Although the value of A will by definition influence the value of ρ_r, no threshold for the void fraction which represents the underside of the roller area has been proposed. In practice, A and ρ_r are very difficult to consistently and accurately measure due to complex hydrodynamics of the aerated region of the breaker (e.g., see *Duncan* [1981], *Govender et al.* [2002], *Kimmoun and Branger* [2007], and the recent review of *Lubin and Chanson* [2017]). The tangent to the smooth water surface below the hydrofoil-generated steady breaker was used by D81 to define A. However, this boundary is much harder to define for developed breakers, for instance forcing *Govender et al.* [2002] to define A as the 'aerated region' only. The difficulty in measuring and defining the roller area has led to the existence of numerous formulations in the literature as shown in Table 2. A simple analysis assuming $H = 1\,\mathrm{m}$, $L_r = 1\,\mathrm{m}$, $\tan\theta = 0.1$, and the beach slope $\tan\beta = 0.01$ demonstrates that it is possible to have an order of magnitude difference between the formulations of D81 and *Tajima* [1996]. This suggests that energy dissipation rates calculated with Eq. 1 can vary by an order of magnitude depending on the choice of A, which likely leads to significant effect for the modelling of the incident wave energy flux through the whole surf zone. Similarly, although cross-shore and temporal variations of ρ_r are expected during the various breaking stages [e.g., see *Blenkinsopp and Chaplin*, 2007; *Kimmoun and Branger*, 2007; *Rojas and Loewen*, 2010], $\rho_r = \rho$ is the common choice in all the previous studies mentioned, which would appear to be a non-physical choice given that this region is characterised by the fact that the flow is two-phase [*Lubin and Chanson*, 2017].

In this paper, we present a novel field dataset of surface roller properties (θ and L_r) extracted from a 2D LiDAR dataset of inner surf zone waves collected by *Martins et al.* [2017a]. The methodology to obtain this dataset is first described and it is then compared to the empirical relations obtained by D81 for steady spilling breakers generated by a hydrofoil. Thanks to these direct measurements of roller properties, the number of unknowns in the parameterization of *Duncan* [1981] (Eq. 1) is reduced to ρ_r and A. We use the classic model of *Svendsen* [1984] and the dissipation term given by *Duncan* [1981] to investigate the capacity of various formulations of A for predicting the energy dissipation rates observed in our inner surf zone data. The role of ρ_r in particular in the definition of A is also discussed in this analysis. Finally, we present an attempt to scale the energy dissipation in the inner surf using local wave properties, which is less reliant on wave geometric properties and could easily be implemented in a phase-averaged model or used by remote-sensing techniques to estimate energy dissipation in broken waves.

156 **Table 1.** List of symbols.

Symbol	Description	Unit
α	mean wave angle relative to shore normal	$^\circ$
β	beach angle with horizontal	$^\circ$
γ	wave height to water depth ratio	–
ϵ	wave energy dissipation due to breaking	$\mathrm{J.m^{-2}}$
η	free surface elevation	m
θ	roller angle	$^\circ$
ρ	water density	$\mathrm{kg.m^{-3}}$
ρ_r	mean water density over the roller area region	$\mathrm{kg.m^{-3}}$
$\overline{\tau}$	period-averaged shear stress at the wave/roller interface	$\mathrm{N.m^{-2}}$
A	roller area	$\mathrm{m^2}$
b	energy dissipation coefficient	–
c	wave celerity	$\mathrm{m.s^{-1}}$
D	wave energy dissipation rate due to breaking	$\mathrm{J.m^{-2}.s^{-1}}$
g	acceleration of gravity	$\mathrm{m.s^{-2}}$
E_f	incident wave energy flux	$\mathrm{J.m^{-1}.s^{-1}}$
$E_{f,w}$	wave contribution to the incident wave energy flux	$\mathrm{J.m^{-1}.s^{-1}}$
$E_{f,r}$	roller contribution to the incident wave energy flux	$\mathrm{J.m^{-1}.s^{-1}}$
H	wave height	m
H_s	significant wave height	m
h	mean water depth	m
h_t	water depth below the trough	m
h_c	water depth below the crest	m
h_w	period-averaged water depth	m
k	wave number	$\mathrm{m^{-1}}$
L	wave length	m
L_r	roller length	m
t	time	s
T	wave period	s
T_p	wave peak period	s
x	horizontal coordinate	m
z	vertical coordinate	m

157 **Table 2.** List of expressions for the surface roller area A from existing literature. Except when stated, all
158 wave and surface roller properties are defined in Figure 1.

Studies	Expression	Observations
Duncan [1981]	$A = 0.11\left(\frac{L_r}{\cos\theta}\right)^2$	Relation found during the hydrofoil experiments. Note that the horizontal projection of the roller/wave interface is used here (L_r), hence the presence of the cosine.
Engelund [1981]	$A = \frac{H^3}{4h\tan\theta}$	This relation was derived by *Deigaard et al.* [1991] to match the dissipation of a hydraulic jump of the same height, based on the results of *Engelund* [1981].
Svendsen [1984]	$A = 0.9H^2$	Based on the reanalysis of *Duncan* [1981].
Okayasu et al. [1986]	$\frac{A}{HL} = 0.06 - 0.07$	L is the wave length. A coefficient k exists in the original version to account for the bore development ($k = 1$ here since we consider fully developed bores).
Tajima [1996]	$A = B\tan\beta H_*^2$	B is a coefficient taken as 140 in *Tajima* [1996], and H_*^2 the equivalent linear wave height (i.e. same energy flux).

2 Methods

2.1 Field site and experimental set-up

The present study uses LiDAR data collected during the field experiments performed at Saltburn-by-the-Sea, UK (see Figure 2a for location) during April 2016 [*Martins et al.*, 2017a,b]. The field experiments and the raw data processing are described in these two references, but some basic information is repeated here. Three eye-safe 2D LiDAR scanners (SICK LMS511) were deployed along a pier to measure the time-varying free surface elevation of shoaling and breaking waves at 25 Hz (Figure 2b). The three individual datasets were processed following the methods of *Martins et al.* [2016] and then merged into a unique surface elevation dataset using linear weighting functions: at a given cross-shore location, priority is given to the nearest LiDAR scanner as it provides the most accurate measurement at that location. An example of the final LiDAR dataset is also shown in Figure 2c and illustrates the spatial resolution and extent of the dataset (0.1-m cross-shore grid). In addition to the scanners, the full experimental set-up included three RBR pressure transducers (PT) and three Nortek Acoustic Doppler Velocimeters (ADV), sampled at 2 Hz and 16 Hz respectively (Figure 2c).

As a consequence of the macrotidal environment in this part of the North Sea, every phase of the nearshore wave transformation could be measured: from propagating bores in the inner surf zone during flood or ebb phases to shoaling and breaking waves during high tides. The present study focuses on the inner surf zone, where broken waves propagate as fully developed bores after the transition point [*Svendsen*, 1984; *Basco and Yamashita*, 1986; *Nairn et al.*, 1990; *Kweon and Goda*, 1996]. We only use data from the 09/04/2016 and 10/04/2016 which corresponded to a swell event with $T_p \approx 10 - 11$ s and $H_s = 1$ m measured at the offshore limit of the pier and had a mean peak wave direction of 16.8°NE and a directional spread of 15.2° at Whitby (Figure 2a). During this period incident waves propagated shore-normal (parallel to the pier), as the coastline of Saltburn is oriented 18°NE. To minimize the influence of reflected waves on the geometrical properties of incident waves, we considered only periods when the maximum runup position was located seaward of the steep gravel upper beachface located around $x = 195$ m (see Figure 2c).

2.2 Wave-by-wave analysis: extraction of roller properties

The surface roller properties presented in this paper are extracted from individual broken waves that are tracked in the inner surf zone using the algorithms developed in *Martins et al.* [2016, 2017c,a,b]. The tracking works by detecting the wave crests as maxima in the surface elevation timeseries. Individual wave heights H are then computed as the vertical distance between the crest and preceding trough elevations (h_c and h_t respectively, see Figure 1), and the wave period T is defined as the time elapsed between the passage of the two troughs either side of a crest at a given cross-shore location. In the LiDAR dataset, we define the surface roller as the part of the wave profile from the wave crest, through the breaking region (where $\partial\eta/\partial x < 0$) to the roller toe. The horizontal distance between the roller toe and the wave crest corresponds to the roller length L_r. For fully developed bores, the roller toe location will be close to and seaward of the preceding trough. Here we use a surface gradient up-crossing value set at 20% of the maximum surface elevation gradient absolute value found in the breaking region to define the roller toe (see illustration in Figure 1). This threshold value was chosen after visually checking every wave of the dataset: smaller threshold values led to the roller toe being located very close to the detected trough that can sometimes be well in front of the roller itself, while larger gradient threshold values led to the detection of the roller toe over the breaking region of the roller, thus underestimating the roller length L_r. Finally, the roller angle θ is estimated by fitting a line to the surface roller profile (from the detected wave crest to the roller toe). We hence make the assumption that, in the inner surf zone, the internal structure of the

roller has a slope similar to that of the surface of the breaking region, which is consistent with observations [e.g., *Duncan*, 1981; *Kimmoun and Branger*, 2007] and the comparisons of A presented in Section 3.2.

In the surf zone, good estimates of the wave celerity are required to accurately describe the incident wave energy flux [*Svendsen et al.*, 2003]. The traditional approach for estimating the wave celerity c relies in the following estimate: $c \approx \Delta x/\Delta t$ where Δx is the distance travelled by the wave in the time Δt [e.g., see *Suhayda and Pettigrew*, 1977]. The Radon Transform [*Radon*, 1917] has also been used to estimate individual wave celerities in video timestacks by *Yoo et al.* [2011] and then *Almar et al.* [2014]. As these methods can introduce considerable noise, which has a dramatic effect in a modelling exercise, we follow the approach of *Tissier et al.* [2015] which makes use of the high-resolution character of the dataset. A linear fit of the crest trajectories is first performed over a 5 m window (2.5 m either side of the point where the celerity is estimated) and the first derivative of this fit is taken as the individual wave celerity.

2.3 The surface roller dataset

The relations obtained by D81 during his hydrofoil experiments are commonly applied in the surf zone to estimate wave energy dissipation [e.g., *Haller and Catalán*, 2009; *Carini et al.*, 2015; *Flores et al.*, 2016], even though their applicability in this region remains unclear due to the mechanism used to generate the steady breakers. In this Section, we present the full dataset that consists of 38 manually selected waves and was obtained with the methodology described in Section 2.2. This dataset is then compared with three empirical relations from D81.

The 38 waves were individually checked and selected to ensure no gaps in the surface elevation dataset and no obvious interaction with other incident or reflected waves. One of these tracked waves is presented in Figure 3 to illustrate the methodology used to extract the roller angle. We first note that the observed range of roller angles is 2 to 6 times greater than the constant value of 5.7° ($\tan\theta \approx 0.1$) typically used by previous investigators in energy balance-based models with the roller concept. These values are consistent with the visual observations reported by *Duncan* [1981], *Govender et al.* [2002] and *Almar et al.* [2012] or those used in Boussinesq-type models [*Schäffer et al.*, 1993; *Cienfuegos et al.*, 2010; *Michallet et al.*, 2011]. Furthermore, θ varies considerably in the inner surf zone (Figures 3a and 3e): a rapid initial reduction in roller angle from 25° to 18° occurs in the first 8 m post-breaking. This is followed by a period of relatively constant roller angle in the range 16° to 22° between $x = 131$ and 160 m, followed by a rapid reduction between $x = 165$ and $x = 170$ m of about 10° associated with an increase in the rate of wave height decay (Figure 3b). This corresponds to the location where the beach slope is the greatest, as seen in the evolution of h_t in Figure 3b. The general trend over the passage of the wave is that high roller angles coincide with greater dissipation, which is evidenced by a more rapid reduction of H (see Appendix for the relation between H and the wave energy flux E_f in the present dataset). Interestingly, we note a delay between high roller angle and high roller length values: local peaks in L_r (e.g. $x = 127$ m and $x = 169$ m) appear 5 to 7 m after those observed in θ ($x = 120$ m and $x = 164$ m, respectively). This highlights the unsteadiness of breaking waves in a natural environment in contrast to the steady-state spilling breakers generated and observed by D81.

As is commonly observed in the inner surf zone [e.g., *Thornton and Guza*, 1982], every wave from the present dataset is found to be depth-limited with a correlation $r^2 = 0.87$ between the individual wave height H and the period-averaged water depth h_w (Figure 4a). In a first attempt to parameterize the roller angle, θ is compared with the wave height (Figure 4b), and the product $L_r \tan\theta$ is shown against the surf zone similarity parameter (Figure 4c). There appears to be a linear trend between $\tan\theta$ and H, however, more data

from other sites and with different conditions are required to establish robust relations between θ and local wave and beach parameters.

Figure 4 d-f show comparisons with the relations provided by D81 concerning the evolution of H with three principal quantities: c^2/g for the dispersive effects (Figure 4d), L_r and $L_r \tan\theta$ for the geometric properties (Figures 4e and f, respectively). We observe that the relation $H = 0.6c^2/g$ derived by D81 consistently overestimates our observations (Figure 4d). The steady-state breakers generated by D81 had a propagation speed imposed by the displacement of the hydrofoil whereas, in the surf zone, amplitude dispersion is generally observed to be important due to increasing wave non-linearities [e.g., *Svendsen et al.*, 1978; *Catalán and Haller*, 2008; *Tissier et al.*, 2011]. To verify this effect on the present dataset, the non-linear wave celerity predictor of *Booij* [1981] was tested:

$$\frac{c_{Booij}^2}{g} = \frac{1}{k}\tanh\left(k\left(h_w + \frac{H}{2}\right)\right), \tag{2}$$

where k is the wave number. In shallow water, the hyperbolic tangent can be approximated as follows (error <0.7% for the present dataset):

$$\frac{c_{Booij}^2}{g} \approx h_w + \frac{H}{2} \tag{3}$$

Using the linear relation found between H and h_w (Figure 4a), we obtain the simple linear relation:

$$\frac{c_{Booij}^2}{g} \approx 2.49H - 0.06 \tag{4}$$

Accounting for the wave non-linearity in the celerity provides a much better estimate of the observed c^2/g than with the formulation of D81, reducing the root-mean square error ($RMSE$) from 0.86 to 0.25 m/s and the scatter index (SI) from 1.74 to 0.21.

The observed values of roller length L_r are relatively well correlated with the wave height ($r^2 = 0.62$), and are slightly larger than that predicted by the relation $L_r = 2.91H$ from the dataset of D81 (Figure 4e). Part of the dataset from *Haller and Catalán* [2009] follows the relation found by D81 and hence the present dataset. However, some of their observations had a notably smaller roller length for a given wave height than the current data when obtained close to the break point, where the roller is not yet fully developed [*Haller and Catalán*, 2009]. The fully developed character of the present roller dataset is confirmed in the comparison of H with $L_r \tan\theta$ (Figure 4f): a simple analysis of the roller geometry (Figure 1) shows that if L_r is correctly measured, we should get $L_r \tan\theta \approx H$. This is verified in the present dataset with $r^2 = 0.89$, a $RMSE$ of 0.06 m and SI of 0.13, showing that the procedure for the extraction of the roller length and angle is robust. In contrast, the surface roller covered only a fraction of the wave face during the hydrofoil experiments performed by D81 (see Figures 1 and 3 in Duncan, 1981) leading to relatively shorter roller lengths, which follow $H = 1.6L_r \tan\theta$. This also explains the greater values of L_r obtained in Figure 4e compared to the relation of D81.

In conclusion, the present dataset differs from that of D81 in three main areas:

- The unsteadiness of natural surf zone processes. This causes delays in the evolution of roller properties with local beach properties and hence dissipation regimes (Figure 3).
- The celerity imposed by the hydrofoil in D81. This contrasts with surf zone data where amplitude dispersion is important (Figure 4d).
- The non-saturated character of the breakers in D81 compared to the fully developed bores from the present dataset (Figure 4f).

3 Modelling energy dissipation rates in broken waves with a roller model

The novel surface roller dataset presented in Section 2 allows the number of unknowns in the parameterization of *Duncan* [1981] (Eq. 1) to be reduced to A and ρ_r only. In this Section, we use this dataset and the roller concept initially developed by *Svendsen* [1984] with the dissipation term from *Duncan* [1981] to investigate the influence of different formulations of A and the role of ρ_r on the modelling of the incident wave energy flux. We first describe the model and the assumptions upon which it is based.

3.1 Model description

3.1.1 The roller model: derivation and assumptions

The concept of energy balance for nearshore wave modelling states that the spatial variation of the time-averaged incident wave energy flux E_f is equal to the amount of energy D (> 0 by convention) transformed or directly dissipated per unit area as discussed by *Svendsen* [2006] (e.g., by breaking, aeration and friction). If x represents the cross-shore coordinate, this model can be expressed as:

$$\frac{\partial}{\partial x}\left(E_f \cos\alpha\right) = -D \tag{5}$$

where α is the mean wave angle relative to shore normal. For waves propagating in the inner surf zone, all of the energy transformed by breaking processes is assumed to be transferred to the surface roller [e.g., *Dally and Brown*, 1995; *Michallet et al.*, 2011], which is a turbulent mass of mixed water and air centred on the Mean Water Level (MWL), and moves at the same speed c as the carrier wave [*Svendsen*, 1984]. To account for the extra kinetic energy present in the roller, S84 separated the incident wave energy flux into a wave and a roller contribution as follows:

$$E_f = E_{f,w} + E_{f,r} \tag{6}$$

with

$$E_{f,w} = \rho g c \frac{1}{T}\int_0^T \eta^2 dt \tag{7}$$

$$E_{f,r} = \frac{1}{2}\rho_r \frac{A}{T} c^2 \tag{8}$$

where ρ is the water density, g is the gravity constant, T is the wave period, η is the time-varying surface elevation, and ρ_r and A the surface roller mean density and area (see also *Deigaard and Fredsøe* [1989]). In practice, the surface roller constitutes the rotational part of the broken wave and accounts for the extra kinetic energy found in breaking and broken waves, see *Svendsen* [1984], *Battjes* [1988], and also the description of the roller model in *Buckley et al.* [2015]. Indeed, the term $E_{f,r}$ represents the kinetic energy of the surface roller and the term $E_{f,w}$ represents twice the wave energy flux calculated from the potential energy of the wave. The hypothesis that the kinetic energy equals the potential energy is hence made for the irrotational part of the wave, and although this assumption has not been thoroughly verified in the inner surf zone for a wide range of wave and beach conditions, the experimental studies of *Iwata and Tomita* [1992] and *Huang et al.* [2009] corroborate these hypotheses.

In Eq. 5, we neglect wave directionality as individual waves were observed to propagate parallel to the pier, and this is confirmed by the small directional spreading measured nearshore. For instance, a wave angle of 10° causes an underestimation of the individual wave energy flux of about 2%, which is considered negligible compared to the approximations of the current model. Further, we focus on inner surf zone waves and hence neglect contributions to the dissipation such as that from air entrainment which are known to be significant in the outer surf zone but whose effect is diminished in the inner surf zone

[e.g., see *Blenkinsopp and Chaplin*, 2007]. The contribution from bottom friction is also neglected as it was found to be negligible on sandy beaches compared to that by breaking processes [e.g., see *Boers*, 2005].

The growth of the surface roller is compensated by the energy dissipation D_τ that occurs through shear stresses at the wave/roller interface and the dissipation that originates from mass exchanges between the wave and the roller [*Nairn et al.*, 1990; *Deigaard*, 1993; *Stive and de Vriend*, 1994; *Reniers and Battjes*, 1997]. *Deigaard* [1993] (see also the note in *Stive and de Vriend* [1994]) showed that the contribution of the mass exchanges to the energy dissipation is similar to the spatial variation of the roller kinetic energy so that with the assumptions made above, we can write:

$$D = D_\tau + \frac{\partial E_{f,r}}{\partial x} \tag{9}$$

The energy balance system from Eq. 5 hence simplifies to a single differential equation:

$$\frac{\partial E_{f,w}}{\partial x} + 2\frac{\partial E_{f,r}}{\partial x} = -D_\tau \tag{10}$$

3.1.2 Energy dissipation terms

From his hydrofoil experiments, D81 related the energy dissipation in steady breakers to the Reynolds stresses at the boundary between the roller and the underlying layers of fluid (see Eq. 1). The dissipation term due to shear stresses corresponds to the work done by the roller averaged over the wave period see also Eq. 1:

$$D_\tau = \overline{\tau c} = \rho_r g A \frac{\sin\theta}{T} \tag{11}$$

In the following, we will also use the original model of *Svendsen* [1984] as a reference:

$$\frac{\partial E_{f,w}}{\partial x} + \frac{\partial E_{f,r}}{\partial x} = -D_{HJ}, \tag{12}$$

The approach of S84 follows the seminal work of *Le Méhauté* [1962] on non-saturated breakers, and that of *Svendsen et al.* [1978] to approximate the energy dissipation in a broken wave with that of a hydraulic jump of the same height such that:

$$D_{HJ} = \frac{1}{4}\rho g h_w \frac{H^3}{h_c h_t T} \tag{13}$$

where h_w is the period-averaged water depth, and h_c and h_t are the water depths below crest and trough respectively [e.g., *Svendsen*, 2006, p. 286], see Figure 1.

3.1.3 Numerical discretization

A and ρ_r are the only unknowns in the description of the kinetic energy of the roller and hence in D_τ. The dataset presented in Section 2 thus enables us to investigate the accuracy of formulations of A (Table 2) and the role of ρ_r to model the amount of energy transformed during the breaking processes and then dissipated at the interface between the roller and the wave. The lack of knowledge of A prevents us to impose a correct boundary condition in the inner surf zone and thus model $E_{f,r}$ directly by using the measured $\partial E_{f,w}/\partial x$ quantities. Instead, here we investigate the validity of the choices of A and ρ_r by modelling $E_{f,w}$ and comparing it to our observations. Eq. 10 and 12 are solved numerically with a finite difference modelling approach to estimate the cross-shore variation of $E_{f,w}$ (Eq. 7) and $E_{f,r}$ (Eq. 8). Starting at an initial position x_0, the model uses measured wave quantities (H, c, θ and L_r) and local quantities (h_w, h_t) to compute the roller contribution and the energy dissipation terms D_τ (Eq. 11) and D_{HJ} (Eq. 13) to feed into Eq.

10 and Eq. 12 respectively. At any cross-shore location x_i, the discretization used for Eq. 9 reads:

$$(E_{f,w})_i = (E_{f,w})_{i-1} - \delta x (D_\tau)_i - 2(E_{f,r})_i + 2(E_{f,r})_{i-1} \tag{14}$$

where the subscripts i and $i-1$ refer to the evaluation of the quantity at the successive grid points x_i and x_{i-1} respectively. $\delta x = x_i - x_{i-1}$ is the spatial discretization step, taken here as 0.1 m. This numerical scheme introduces a local error of $O(\delta x^2)$, meaning that the numerical method is of order 1 over the whole surf zone. This is considered satisfactory for the present application considering approximations made in the roller concept.

3.2 Influence of A and ρ_r on energy dissipation rates

For the following analysis, a wave group composed of 6 consecutive waves was isolated to highlight the effect of A and ρ_r on the cross-shore evolution of $E_{f,w}$ modelled with Eq. 14. More information on this group is given in the Appendix. The wave and roller properties of this group were extracted using the methodology presented in Section 2.2 and ensemble-averaged.

The basic analysis on the order of magnitude of A presented in Section 1 showed potential for large discrepancies between the different formulations presented in Table 2. The roller properties extracted from the wave group here confirm this analysis (Figure 5), and show that the formulations of *Tajima* [1996] and *Okayasu et al.* [1986] lead to values approximately 6 and 10 times larger respectively than those of *Engelund* [1981], when the original coefficients for these formulations are used. Although the relation found by S84 is based on the dataset obtained by D81, it consistently predicts a smaller roller surface area than the original relation of D81. The difference between the two formulations increases slightly closer to shore, where L_r tends to get larger in our observations than the quantity $2.91H$ observed by D81 (Figure 4e). The roller area model derived by *Deigaard and Fredsøe* [1989] and *Deigaard et al.* [1991] to match the dissipation rates of a hydraulic jump of the same height (based on *Engelund* [1981]) gives the smallest estimates of A: roughly half that of S84 and a third of D81.

The variability in values of A obtained by using different formulations lead to differences of the same order in the roller kinetic energy (Eq. 8) and likely in its cross-shore variation which is the quantity used by the model. More importantly, the dissipation terms D_τ (Eq. 11) computed with these formulations will also show such variations depending on the choice made for A. For instance, using the formulation by *Okayasu et al.* [1986] leads to energy dissipation rates about 10 times greater than given by *Engelund* [1981] (Table 2). Considering the number of studies that have estimated the energy dissipation rates to be close to that of a bore, and that the formulations from *Tajima* [1996] and *Okayasu et al.* [1986] are not supported by observations, in the following, we focus our attention on the formulations by *Engelund* [1981], *Duncan* [1981] and *Svendsen* [1984].

Starting with the formulation by *Engelund* [1981], the best fit with observations is obtained with a density ratio of $\rho_r/\rho = 0.87$ (Figure 6b), corresponding to a $RMSE$ of $57.32\,\mathrm{J.m^{-1}.s^{-1}}$. It is important to note that due to the absence of definition for A, there is a lack of knowledge on ρ_r. However, the value of 0.87ρ is well within the range of previous observations of void fractions in the roller region of inner surf zone waves [*Longuet-Higgins and Turner*, 1974; *Duncan*, 1981; *Cox and Shin*, 2003; *Kimmoun and Branger*, 2007; *Govender et al.*, 2002; *Rojas and Loewen*, 2010]. As an energy dissipation at least twice that of a hydraulic jump of the same height is observed for the original formulations of roller area from D81 and S84, a modification to the coefficients of these formulations is required to match our observations. Here, we propose to include the density ratio in these new coefficients. This is motivated by two reasons: 1) these coefficients will change depending on the chosen value for ρ_r, and 2) A and ρ_r are directly linked through the definition of A. The modified roller area formulations of *Duncan* [1981] and *Svendsen* [1984]

for this specific wave group are given by:

$$A = 0.026\frac{\rho}{\rho_r}\left(\frac{L_r}{\cos\theta}\right)^2 \quad \text{modified from } \textit{Duncan} \text{ [1981]} \tag{15}$$

$$A = 0.326\frac{\rho}{\rho_r}H^2 \quad \text{modified from } \textit{Svendsen} \text{ [1984]} \tag{16}$$

To be consistent with the results obtained with the formulation of *Engelund* [1981], the same mean roller density is taken, meaning that the modified roller areas represent 27% and 42% of the original formulations of D81 and S84 respectively. As the coefficients of Eq. 15 and 16 are prone to change with the accuracy of the estimation of wave and roller properties, the values were also computed for a less energetic wave group leading to a similar coefficient for Eq. 15 but a slightly larger value for Eq. 16 (0.362). Performing the same analysis over the 38 individual waves led to a mean value of 0.364 and a standard deviation of 0.059 which is consistent with the wave group values. Further studies could investigate the variability of these coefficients to wave conditions and beach types. For the present analysis, we focus on the wave group that led to the coefficients of Eq. 15 and 16.

Between $x = 122$ and 135 m, Eq. 16 gives the best match with data (Figure 6b), with energy dissipation rates very similar to those of a hydraulic jump of the same height, D_{HJ} (Eq. 13), see Figure 6a. By contrast, Eq. 15 and the formulation of *Engelund* [1981] lead to energy dissipation rates on average 5 J.m^{-2}.s^{-1} smaller than that given by Eq. 15 which explains the discrepancies observed between $E_{f,w}$ modelled with these two formulations and the data around $x = 140$ m. Landward of this cross-shore position however, the modified formulation of S84 (Eq. 16) predicts energy dissipation rates on average 2-3 J.m^{-2}.s^{-1} lower than D_{HJ} and that of D81 (Eq. 15) which remains similar to D_{HJ} (Figure 6a). Overall, this has a direct impact on the cross-shore modelling of $E_{f,w}$: very good results are obtained with the formulation from Eq. 16 ($RMSE = 38.82$ J.m^{-1}.s^{-1}), which succeeds in capturing the change in dissipation regime mentioned above, whereas Eq. 15 correctly estimates the total dissipation over the inner surf zone ($RMSE$ of 60.18 J.m^{-1}.s^{-1}) but is less accurate in capturing the two different dissipation regimes described above. It is worth noting that the original formulation of *Duncan* [1981] was changed to match the observations over the whole domain studied here. By slightly increasing the coefficient in Eq. 15, it is possible to better describe $E_{f,w}$ in the first section ($x = 122$ to 140 m), however, the description of the overall energy dissipation rates would be incorrect as it would lead to large discrepancies around $x = 170$ m.

Although the roller areas estimated using Eq. 15 and 16 are similar, the term $2\partial E_{f,r}/\partial x$ computed using these equations differs (Figure 6c). The measured roller lengths exhibit higher spatial variation when compared to the wave height, which means that Eq. 15 leads to spatial oscillations with higher amplitudes. In this comparison, it is also worth noting that the spatial variation of $2E_r$ oscillates around 0, meaning that there is an overall steady state reached characteristic of inner surf zone waves. Although the roller contribution to wave setup is small compared to other processes [*Apotsos et al.*, 2007], the influence of the new formulations in the estimation of wave setup and the mean circulation of the surf zone needs to be further investigated in both 2DH and 3D circulation models, as the wave-induced mixing and vertical circulation is an important component for wave setup [*Bennis et al.*, 2014; *Guérin et al.*, 2018].

To conclude this Section, it is noted that D81 required a value of $\rho_r = 0.61\rho$ to match his theory with observations. When a density ratio of 0.61 is used for the roller, the original formulation of D81 for A leads to values 2.58 times greater than those required to match our observations. With the original formulation of D81, a value of $\rho_r = 0.23\rho$ is required to match the current observations which would appear to be unrealistic in the inner surf zone [e.g., see *Kimmoun and Branger*, 2007]. To illustrate the effect of ρ_r on the roller area A for the current dataset, Figure 7 presents a visual comparison of the roller areas computed from Eq. 16 using mean roller density ratios of 0.8 and 0.4 alongside that cal-

culated using D81 with $\rho_r/\rho = 0.23$. Due to the clear physical link between the definition of the roller area and the value of the mean roller density, a study combining the analysis above with new laboratory measurements of the roller structure in inner surf zone waves would be beneficial.

4 Scaling wave breaking energy dissipation in the inner surf zone

The previous section demonstrated that accurate roller properties are necessary to correctly predict the energy dissipation in inner surf zone waves using roller-based models. However, some of the assumptions used in this model, such as on the amount of energy transferred by the breaking wave to the roller, are commonly used but have not been robustly verified. Considering the complex interactions and exchanges observed at the wave/roller interface, we can also consider the parameterizations of the energy dissipation in broken waves through shear stresses only (Eq. 11) a simplification of the complex processes occurring in broken waves. For instance, the interaction between turbulent surf zone flows and incident waves [*Teixeira and Belcher*, 2002] or the generation of turbulence by wave breaking [e.g., see *Nairn et al.*, 1990] are very often neglected, simplified or hidden in the dissipation terms (e.g. with Eq. 12). Further, the practical use of roller-based models is hampered by the lack of parameterizations for roller properties, meaning that there is a need for alternative parameterizations of the energy dissipation due to breaking which rely less heavily on a priori unknown parameters. By analysing the deficit in momentum behind hydrofoil generated breakers, D81 was the first to express the energy dissipation per unit area as a simple function of the wave celerity to the fifth power:

$$\epsilon = b\rho\frac{c^5}{g} \tag{17}$$

where b is a dissipation coefficient of the form $\alpha/\sin\theta$ (where α is a constant), which takes values in the range 0.031 to 0.066 in the dataset of D81. Later, *Melville* [1994] found lower values of b in the range 0.004 to 0.012 for focussed deep water laboratory waves, with b increasing with the wave steepness. Interestingly, a simple approximation of the hydraulic jump energy dissipation rate [with $c \sim 1.14\sqrt{gh}$, *Tissier et al.*, 2011] leads to:

$$\epsilon_{HJ} \sim 1/4\rho g\frac{H^3}{h}c = 1/4\rho\frac{H^3}{h^3}\frac{g^2h^2}{g}c \sim \rho\frac{\gamma^3}{5.2}\frac{c^5}{g}, \tag{18}$$

where γ is the wave height to water depth ratio. For the present dataset, Eq. 18 corresponds to b within 0.01 and 0.015, roughly a third of the values from D81, but well within the range of values obtained by *Melville* [1994]. *Drazen et al.* [2008] performed an extensive analysis of several experimental datasets to further understand the variation of this parameter [e.g., *Melville*, 1994; *Drazen et al.*, 2008; *Romero et al.*, 2012], and highlighted the dependence of b on $(Hk)^{5/2}$. It is worth noting that in this expression for b, *Drazen et al.* [2008] defined H as the height of the 'active' or 'overturning' part of the wave, which is equal to H as defined in Figure 1 (fully developed bores in the inner surf zone).

Provided that the break point and wave celerity in inner surf zones are accurately described, the formulation of the energy dissipation rate from Eq. 17 has potential for parameterizing energy dissipation in broken waves in the inner surf zone. While it is a function of the wave steepness, Eq. 17 relies less on surface roller properties which still lack parameterization (e.g. Figure 4). In the following, we investigate the performance of the two formulations for b (D81 and *Drazen et al.* [2008]) to simulate the cross-shore transformation of the wave energy flux at the wave group and wave-by-wave scales. The period-averaged energy dissipation rates given by Eq. 17 is used in Eq. 5 and we use the data from the same wave group as in Section 3. The optimum coefficients found for the formulations of D81 and *Drazen et al.* [2008] when compared to observations (wave group and individual waves) were found to be:

$$b = 1.24(Hk)^{5/2} \qquad \text{modified from } \textit{Drazen et al.} \text{ [2008]} \tag{19}$$

$$b = 0.0011/\sin\theta \qquad \text{modified from } \textit{Duncan} \text{ [1981]} \tag{20}$$

where, k is the wave number and has been calculated using the measured surf zone quantity cT.

The dissipation coefficient b computed with Eq. 19 and 20 for the ensemble averaged wave group (Appendix A1) demonstrates contrasting cross-shore evolution (Figure 8). The formulation of D81 (Eq. 20) predicts b values steadily increasing from 0.003 to 0.005 with decreasing values of $\sin\theta$ as waves approach the beach. By contrast, the formulation of *Drazen et al.* [2008] (Eq. 19) leads to b values that decrease approximately linearly as x increases, although two different phases are noted: a section ($x = 120 - 150$ m) where b has a decreasing trend with large oscillations, and a section ($x = 150 - 170$ m) where b decreases more rapidly. Interestingly, the change occurring around $x = 150$ m corresponds to where the beach slope steepens from about 1 : 80 to about 1 : 30 (Figure 2c and 3b).

The difference in behaviour between Eq. 19 and 20 has a direct impact on the dissipation terms computed with Eq. 18 (Figure 9a). Seaward of $x = 135$ m, Eq. 19 presents energy dissipation rates close to that given by the hydraulic jump theory, while Eq. 20 gives slightly lower rates. Landward of this position, Eq. 19 leads to energy dissipation rates between 5-10 $\mathrm{J.m^{-2}.s^{-1}}$ lower than D_{HJ}, while the difference with D_{HJ} is smaller for Eq. 20 (Figure 9a). Both energy dissipation formulations lead to similar model skills, with $RMSE$ of 41.4 and 39.8 $\mathrm{J.m^{-1}.s^{-1}}$ obtained for Eq. 19 and 20 respectively (Figure 9b). Indeed, both formulations capture the global transformation of incident wave energy flux reasonably well, however, Eq. 19 leads to a better description of $E_{f,w}$ in the region where the dissipation is close to that of a hydraulic jump of the same height (up to $x = 140$ m). The same order of accuracy is obtained at the wave-by-wave scale, see Figure 10. The six waves constituting the wave group are modelled individually and, if we exclude the 5th wave (Figure 10e), the $RMSE$ ranges from 36.5 to 61.9 $\mathrm{J.m^{-1}.s^{-1}}$ when Eq. 19 is used, while it varies from 60 to 126 $\mathrm{J.m^{-1}.s^{-1}}$ when Eq. 20 is used. As the formulation proposed by *Drazen et al.* [2008] suggests that b is a function of $(1/T)^5/2$, we highlight the sensitivity of the model to the individual wave period in Figure 10 by modelling $E_{f,w}$ with $T \pm 1$ s. We note that the effect of an inaccurate individual wave period, which can be difficult to define in the surf zone, induces variations in the modelled energy flux of the order of the noise in the observations.

It is important here to draw the parallel between the greater model skill displayed by Eq. 19 with the best skills in the roller model (Section 3.2) obtained with the formulation for A of *Svendsen* [1984]. Both the dissipation coefficient b from *Drazen et al.* [2008] and the roller area given by *Svendsen* [1984] use the wave height H in their expression. By contrast, Eq. 20 predicts an increasing dissipation coefficient b for decreasing roller angle, which is not observed in the present dataset. This has implications for the parameterizations of energy dissipation rates in surf zone broken waves, e.g. in spectral or probabilistic models. Provided that the local wave height is retrieved correctly from the wave energy flux (see Appendix) and that the wave celerity and break point location are provided accurately, it seems possible to develop simple forward methods to estimate local energy dissipation rates with Eq. 19.

5 Concluding remarks

In this paper, we present a high-resolution LiDAR dataset from which the geometrical properties of surface rollers (θ and L_r) are extracted. This dataset constitutes the first direct measurements of these properties from field experiments. We report roller angle values up to 6 times greater than the value of 5.7° typically used in energy balance-based numerical models that use the parameterization of *Duncan* [1981] to model the energy dissipation in broken waves (Eq. 1 and 11). Future deployment of LiDAR scanners at different field sites will enable this dataset to be extended for a range of wave conditions and beach types, and will potentially allow the parameterization of L_r and θ as a function of wave and beach parameters.

These novel measurements reduce the number of unknowns in the parameterization of D81 (Eq. 11) to the roller area A and the mean roller density ρ_r, which are two parameters linked through the definition of A. This hence allows for a sensitivity analysis of the ability of different formulations for A present in the literature (Table 2) to model energy dissipation rates in broken waves. The results first obtained with the roller area of *Engelund* [1981] show that in the present dataset, broken waves propagating in the inner surf zone were dissipating their energy at a similar, but generally smaller rate ($\rho_r = 0.87\rho$) than hydraulic jumps of the same height. This is consistent with many past observations [e.g., see *Le Méhauté*, 1962; *Hwang and Divoky*, 1970; *Svendsen et al.*, 1978; *Battjes and Janssen*, 1978; *Thornton and Guza*, 1983; *Svendsen*, 1984; *Battjes and Stive*, 1985; *Svendsen et al.*, 2003]. The value $\rho_r = 0.87\rho$ is within the range of previous observations of void fraction in inner surf zone waves [e.g. *Kimmoun and Branger*, 2007], but this mean density corresponds to a surface roller confined in the most aerated part of the breaker (Figure 7), suggesting that a smaller mean roller density is more likely. To be consistent with the definition of ρ_r and account for this uncertainty, we incorporate the mean roller density ratio ρ_r/ρ into modified versions of the formulations for A given by D81 and S84 to yield energy dissipation rates that agree with the present measurements. Indeed, no clear interface between the wave and the roller is generally observable for inner surf zone waves and fully developed bores as it was during the hydrofoil experiments of D81. Additional experiments are required to understand the link between ρ_r and A, and to answer questions such as: is there a void fraction that clearly defines the wave/roller interface or is it only related to the roller hydrodynamics (e.g. the most turbulent region). Further work could also investigate wave setup and undertow, probably in a more controlled environment, as it could lead to a better understanding of A and ρ_r and a better knowledge of the contribution of surface rollers in surf zone mean flow.

The incorporation of ρ_r/ρ into the formulations for A and the uncertainties regarding these two parameters do not alone explain the modification of the original roller area formulation obtained by *Duncan* [1981], and that later derived by *Svendsen* [1984]. Another reason for this lies in the dataset upon which both original formulations were based. Indeed, the results of Section 2.3 suggest that the relations between wave and roller geometrical quantities from the hydrofoil-generated experiments [*Duncan*, 1981] do not necessarily apply in a natural inner surf zone. This is in agreement with the observations made by *Melville* [1994] and *Drazen et al.* [2008] who found greater dissipation in the hydrofoil waves of D81 than in 'classic' unsteady breaking waves, corresponding to higher b values. The reason probably lies in the greater celerity imposed on the hydrofoil-generated wave compared to that of natural unsteady breakers (Figure 4d), which induces greater energy dissipation. Nonetheless, we note that the modified version of the formulation by *Svendsen* [1984] leads to the best prediction of the incident wave energy flux across the inner surf zone.

Finally, a scaling law (Eq. 17) first introduced by *Duncan* [1981] relating the energy dissipation to the wave celerity is tested against our dataset. The dissipation coefficient b given by *Drazen et al.* [2008] appears to accurately describe the wave energy dissipation in the inner surf zone at both wave group and wave-by-wave scales. This is very promis-

ing as this approach could be adopted in spectral models to estimate energy dissipation rates in depth-induced wave breaking regions such as in the inner surf zone. It also has the advantage that it relies less on internal wave properties (in contrast to the roller model) and hence includes all physical processes responsible for the dissipation of energy during breaking. Nonetheless, robust descriptions of the break point location and wave celerity over the whole surf zone are still required [e.g., *Svendsen et al.*, 2003].

A: Energetic properties of the isolated wave group

As part of the present analysis, a wave group consisting of 6 consecutive and similar waves was isolated (see Figure A.1a). In this Appendix, we present this wave group, and give further notes on the use of linear wave theory for describing the energy flux in the surf zone at the group and wave-by-wave scales.

In practice, when H is defined at the wave-by-wave scale (trough to crest distance), the following expression based on linear wave theory should be used for describing the wave energy flux in the shoaling and surf zones

$$E_{f,lin} = \rho g c H^2 B_0, \tag{A.1}$$

where

$$B_0 = \frac{1}{T}\int_0^T \left(\frac{\eta}{H}\right)^2 dt \tag{A.2}$$

The shape parameter B_0 was introduced by *Svendsen* [1984] and *Stive* [1984] (denoted as A_F in the latter) to account for the increase in wave steepness, skewness and then asymmetry generally observed in the profile of surf zone waves. These non-linearities in the wave profile lead to increasing discrepancies between B_0 and 0.125, the value obtained for linear waves [e.g., *Svendsen et al.*, 1978; *Svendsen*, 1983, 1984; *Stive*, 1984; *Basco and Yamashita*, 1986; *Buhr Hansen*, 1990; *Svendsen et al.*, 2003; *Huang et al.*, 2009; *Michallet et al.*, 2011; *Martins et al.*, 2017c].

In shallow water, B_0 is generally found to vary in the cross-shore direction: it is close to 0.125 in the shoaling region [*Basco and Yamashita*, 1986], but rapidly decreases towards the break point and then slowly varies in the inner surf zone to a value close to a typical value of 0.075 due to a more skewed wave profile [*Svendsen*, 1983, 1984; *Basco and Yamashita*, 1986; *Buhr Hansen*, 1990; *Svendsen*, 2006]. For the data presented here, B_0 values for individual waves are smaller than 0.1 and B_0 is typically found to decrease with increasing wave skewness (see example of Figure A.2), where skewness is computed as:

$$S_k = \frac{\overline{(\eta - \overline{\eta})^3}}{\overline{(\eta - \overline{\eta})^2}^{3/2}} \tag{A.3}$$

By combining the observations from Figure A.1 and Eq. A.1, we deduce that B_0 takes the value 0.0625 (1/16) at the wave group scale for the present inner surf zone dataset ($RMSE$ of 12.05 J/unit area between Eq. 7 and Eq. A.1 with this value), which is close to the typical value of 0.075 [*Svendsen*, 1983]. It is worth noting that to retrieve the local wave height from the modelled wave energy flux in the present study (e.g. Section 3.2), Eq. A.1 has to be used with the value $B_0 = 0.0625$. At the wave-by-wave scale, we note more variability; this can be observed in the greater standard deviations obtained with the integral form (Eq. 7). There are two potential reasons for this:

- There can be a great variability in shape from one wave to another (e.g. Figure A.2), and the formulation of Eq. A.1 does not account for the wave length or frequency, nor for the wave breaking 'history', whereas Eq. 7 does.
- Calculating an integral over such a high-resolution dataset is evidently sensitive to the temporal boundaries. Therefore, the location of the individual wave troughs has the potential to affect the amount of energy estimated.

Acknowledgments

The authors would like to acknowledge the financial assistance provided by the Engineering and Physical Sciences Research Council (EP/N019237/1). Kévin Martins was supported by the University of Bath, through a University Research Services (URS) scholarship. Assistance during the field experiments from Jack Puleo, Brittany Bruder and Aline Pieterse (University of Delaware, US), is greatly appreciated. José Beya (Universidad de Valparaíso, Chile) and James Duncan (University of Maryland, MD, US) are greatly acknowledged for fruitful exchanges. We thank two anonymous reviewers for their detailed and constructive comments which made the manuscript improve. The data used in this research are available from the University of Bath Research Data Archive (doi: 10.15125/BATH-00461) and from the corresponding author.

References

Almar, R., R. Cienfuegos, P. A. Catalán, H. Michallet, B. Castelle, P. Bonneton, and V. Marieu (2012), A new breaking wave height direct estimator from video imagery, *Coastal Eng.*, *61*, 42 – 48, doi:10.1016/j.coastaleng.2011.12.004.

Almar, R., H. Michallet, R. Cienfuegos, P. Bonneton, M. Tissier, and G. Ruessink (2014), On the use of the radon transform in studying nearshore wave dynamics, *Coastal Eng.*, *92*, 24 – 30, doi:10.1016/j.coastaleng.2014.06.008.

Apotsos, A., B. Raubenheimer, S. Elgar, R. T. Guza, and J. A. Smith (2007), Effects of wave rollers and bottom stress on wave setup, *J. Geophys. Res. Oceans*, *112*(C2), doi: 10.1029/2006JC003549.

Bae, J. S., H.-J. Kim, and J. Choi (2013), Surface roller effect affecting on shear fluctuations of a SandyDuck experiment under a random wave environment, *Journal of Coastal Research*, *165*, 1491 – 1496, doi:10.2112/SI65-252.1.

Baldock, T. E., P. Holmes, S. Bunker, and P. V. Weert (1998), Cross-shore hydrodynamics within an unsaturated surf zone, *Coastal Eng.*, *34*(3), 173 – 196, doi:10.1016/S0378-3839(98)00017-9.

Basco, D., and T. Yamashita (1986), Toward a simple model of the wave breaking transition region in the surf zones, in *Proceedings of the 20th Conference on Coastal Engineering, Taipei, Taiwan*, pp. 955 – 970.

Basco, D. R. (1985), A qualitative description of wave breaking, *J. Waterway, Port, Coastal, Ocean Eng.*, *111*(2), 171–188, doi:10.1061/(ASCE)0733-950X(1985)111:2(171).

Battjes, J. A. (1988), Surf-zone dynamics, *Ann. Rev. Fluid Mech.*, *20*(1), 257 – 291, doi: 10.1146/annurev.fl.20.010188.001353.

Battjes, J. A., and J. P. F. M. Janssen (1978), Energy loss and set-up due to breaking of random waves, in *Proceedings of the 16th Conference on Coastal Engineering, Hamburg, Germany*, pp. 569 – 587.

Battjes, J. A., and M. J. F. Stive (1985), Calibration and verification of a dissipation model for random breaking waves, *J. Geophys. Res. Oceans*, *90*(C5), 9159 – 9167, doi: 10.1029/JC090iC05p09159.

Bennis, A.-C., F. Dumas, F. Ardhuin, and B. Blanke (2014), Mixing parameterization: Impacts on rip currents and wave set-up, *Ocean Eng.*, *84*, 213 – 227, doi: 10.1016/j.oceaneng.2014.04.021.

Benoit, M., F. Marcos, and F. Becq (1996), Development of a third generation shallow-water wave model with unstructures spatial meshing, in *Proceedings of the 25th Conference on Coastal Engineering, Orlando, Florida*, pp. 465 – 478.

Blenkinsopp, C. E., and J. R. Chaplin (2007), Void fraction measurements in breaking waves, *Proc. R. Soc. A*, *463*(2088), 3151 – 3170, doi:10.1098/rspa.2007.1901.

Boers, M. (2005), Surf zone turbulence, Ph.D. thesis, Technische Universiteit Delft.

Bonneton, P. (2007), Modelling of periodic wave transformation in the inner surf zone, *Ocean Engineering*, *34*(10), 1459 – 1471, doi:10.1016/j.oceaneng.2006.09.002.

Bonneton, P., N. Bruneau, B. Castelle, and F. Marche (2010), Large-scale vorticity generation due to dissipating waves in the surf zone, *Discrete Continuous Dyn. Syst.*, *13*(4), 729 – 738, doi:10.3934/dcdsb.2010.13.729.

Booij, N. (1981), Gravity waves on water with non-uniform depth and current, Ph.D. thesis, Technische Hogeschool, Delft (Netherlands).

Brocchini, M. (2013), A reasoned overview on boussinesq-type models: the interplay between physics, mathematics and numerics, *Proc. R. Soc. A*, *469*(2160), doi:10.1098/rspa.2013.0496.

Brocchini, M., M. Drago, and L. Iovenitti (1992), The modelling of short waves in shallow waters. comparison of numerical models based on boussinesq and serre equations, in *Proceedings of the 23rd Conference on Coastal Engineering, Venice, Italy*, pp. 76 – 88.

Brocchini, M., A. Kennedy, L. Soldini, and A. Mancinelli (2004), Topographically controlled, breaking-wave-induced macrovortices. part 1. widely separated breakwaters, *J. Fluid Mech.*, *507*, 289 – 307, doi:10.1017/S002211200400878X.

Buckley, M. L., R. J. Lowe, J. E. Hansen, and A. R. V. Dongeren (2015), Dynamics of wave setup over a steeply sloping fringing reef, *J. Phys. Oceanogr.*, *45*(12), 3005 – 3023, doi:10.1175/JPO-D-15-0067.1.

Bühler, O., and T. E. Jacobson (2001), Wave-driven currents and vortex dynamics on barred beaches, *J. Fluid Mech.*, *449*, 313 – 339, doi:10.1017/S0022112001006322.

Buhr Hansen, J. (1990), Periodic waves in the surf zone: Analysis of experimental data, *Coastal Eng.*, *14*(1), 19 – 41, doi:10.1016/0378-3839(90)90008-K.

Carini, R. J., C. C. Chickadel, A. T. Jessup, and J. Thomson (2015), Estimating wave energy dissipation in the surf zone using thermal infrared imagery, *J. Geophys. Res. Oceans*, *120*(6), 3937 – 3957, doi:10.1002/2014JC010561.

Catalán, P. A., and M. C. Haller (2008), Remote sensing of breaking wave phase speeds with application to non-linear depth inversions, *Coastal Eng.*, *55*(1), 93 – 111, doi:10.1016/j.coastaleng.2007.09.010.

Cavaleri, L., J.-H. G. M. Alves, F. Ardhuin, A. Babanin, M. Banner, K. Belibassakis, M. Benoit, M. Donelan, J. Groeneweg, T. H. C. Herbers, P. Hwang, P. A. E. M. Janssen, T. Janssen, I. V. Lavrenov, R. Magne, J. Monbaliu, M. Onorato, V. Polnikov, D. Resio, W. E. Rogers, A. Sheremet, J. M. Smith, H. L. Tolman, G. van Vledder, J. Wolf, and I. Young (2007), Wave modelling – the state of the art, *Prog. Oceanogr.*, *75*(4), 603 – 674, doi:10.1016/j.pocean.2007.05.005.

Cienfuegos, R., E. Barthélemy, and P. Bonneton (2010), Wave-breaking model for boussinesq-type equations including roller effects in the mass conservation equation, *J. Waterway, Port, Coastal, Ocean Eng.*, *136*(1), 10 – 26, doi:10.1061/(ASCE)WW.1943-5460.0000022.

Cox, D. T., and S. Shin (2003), Laboratory measurements of void fraction and turbulence in the bore region of surf zone waves, *J. Eng. Mech.*, *129*(10), 1197 – 1205, doi:10.1061/(ASCE)0733-9399(2003)129:10(1197).

Dally, W. R., and C. A. Brown (1995), A modeling investigation of the breaking wave roller with application to cross-shore currents, *J. Geophys. Res. Oceans*, *100*(C12), 24,873 – 24,883, doi:10.1029/95JC02868.

Deane, G. B. (1997), Sound generation and air entrainment by breaking waves in the surf zone, *J. Acoust. Soc. Am.*, *102*(5), 2671–2689, doi:10.1121/1.420321.

Deigaard, R. (1993), A note on the three-dimensional shear stress distribution in a surf zone, *Coastal Eng.*, *20*(1), 157 – 171, doi:10.1016/0378-3839(93)90059-H.

Deigaard, R., and J. Fredsøe (1989), Shear stress distribution in dissipative water waves, *Coastal Eng.*, *13*(4), 357 – 378, doi:10.1016/0378-3839(89)90042-2.

Deigaard, R., P. Justesen, and J. Fredsøe (1991), Modelling of undertow by a one-equation turbulence model, *Coastal Eng.*, *15*(5), 431 – 458, doi:10.1016/0378-3839(91)90022-9.

Deike, L., W. K. Melville, and S. Popinet (2016), Air entrainment and bubble statistics in breaking waves, *J. Fluid Mech.*, *801*, 91 – 129, doi:10.1017/jfm.2016.372.

Drazen, D. A., W. K. Melville, and L. Lenain (2008), Inertial scaling of dissipation in unsteady breaking waves, *J. Fluid Mech.*, *611*, 307 – 332, doi: 10.1017/S0022112008002826.

Duncan, J. H. (1981), An experimental investigation of breaking waves produced by a towed hydrofoil, *Proc. R. Soc. A*, *377*(1770), 331 – 348, doi:10.1098/rspa.1981.0127.

Engelund, F. (1981), A simple theory of hydraulic jumps, *Tech. rep.*, Inst. Hydrodyn. Hydraul. Eng. (ISVA), Tech. Univ. Denmark, Progress Rep, 54: 29 – 32.

Flores, R. P., P. A. Catalán, and M. C. Haller (2016), Estimating surfzone wave transformation and wave setup from remote sensing data, *Coastal Eng.*, *114*, 244 – 252, doi: 10.1016/j.coastaleng.2016.04.008.

Govender, K., G. P. Mocke, and M. J. Alport (2002), Video-imaged surf zone wave and roller structures and flow fields, *J. Geophys. Res. Oceans*, *107*(C7), 9–1 – 9–21, doi: 10.1029/2000JC000755.

Guérin, T., X. Bertin, T. Coulombier, and A. de Bakker, (2018), Impacts of wave-induced circulation in the surf zone on wave setup, *Ocean Model.*, *123*, 86 – 97, doi: 10.1016/j.ocemod.2018.01.006.

Haller, M. C., and P. A. Catalán (2009), Remote sensing of wave roller lengths in the laboratory, *J. Geophys. Res. Oceans*, *114*(C7), doi:10.1029/2008JC005185, c07022.

Higuera, P., J. L. Lara, and I. J. Losada (2013), Realistic wave generation and active wave absorption for Navier-Stokes models: Application to OpenFOAM®, *Coastal Eng.*, *71*, 102 – 118, doi:10.1016/j.coastaleng.2012.07.002.

Huang, Z.-C., S.-C. Hsiao, H.-H. Hwung, and K.-A. Chang (2009), Turbulence and energy dissipations of surf-zone spilling breakers, *Coastal Eng.*, *56*(7), 733 – 746, doi: 10.1016/j.coastaleng.2009.02.003.

Hwang, L.-S., and D. Divoky (1970), Breaking wave setup and decay on gentle slopes, in *Proceedings of the 12th Conference on Coastal Engineering, Washington, D.C.*, pp. 377 – 389.

Iafrati, A. (2011), Energy dissipation mechanisms in wave breaking processes: Spilling and highly aerated plunging breaking events, *J. Geophys. Res. Oceans*, *116*(C7), doi: 10.1029/2011JC007038.

Iwata, K., and T. Tomita (1992), Variation of potential and kinetic wave energy in the surf zone, in *Proceedings of the 23rd Conference on Coastal Engineering, Venice, Italy*, pp. 336 – 349.

Jacobsen, N. G., D. R. Fuhrman, and J. Fredsøe (2012), A wave generation toolbox for the open-source CFD library: OpenFoam®, *Int. J. Numer. Methods Fluids*, *70*(9), 1073 – 1088, doi:10.1002/fld.2726.

Kennedy, A. B., Q. Chen, J. T. Kirby, and R. A. Dalrymple (2000), Boussinesq modeling of wave transformation, breaking, and runup. I: 1D, *J. Waterway, Port, Coastal, Ocean Eng.*, *126*(1), 39 – 47, doi:10.1061/(ASCE)0733-950X(2000)126:1(39).

Kimmoun, O., and H. Branger (2007), A particle image velocimetry investigation on laboratory surf-zone breaking waves over a sloping beach, *J. Fluid Mech.*, *588*, 353 – 397, doi:10.1017/S0022112007007641.

Klonaris, G. T., C. D. Memos, and N. K. Drønen (2016), High-order boussinesq-type model for integrated nearshore dynamics, *J. Waterway, Port, Coastal, Ocean Eng.*, *142*(6), 04016,010, doi:10.1061/(ASCE)WW.1943-5460.0000349.

Kweon, H.-M., and Y. Goda (1996), A parametric model for random wave deformation by breaking on arbitrary beach profiles, in *Proceedings of the 25th Conference on Coastal Engineering, Orlando, Florida*, pp. 261 – 274.

Lannes, D., and P. Bonneton (2009), Derivation of asymptotic two-dimensional time-dependent equations for surface water wave propagation, *Physics of Fluids*, *21*(1), 016,601, doi:10.1063/1.3053183.

Le Méhauté, B. (1962), On non-saturated breakers and the wave run-up, in *Proceedings of the 12th Conference on Coastal Engineering, Mexico City, Mexico*, pp. 77 – 92.

Lin, P., and P. L.-F. Liu (1998), A numerical study of breaking waves in the surf zone, *J. Fluid Mech.*, *359*, 239 – 264, doi:10.1017/S002211209700846X.

Lippmann, T. C., A. H. Brookins, and E. B. Thornton (1996), Wave energy transformation on natural profiles, *Coastal Eng.*, *27*(1), 1 – 20, doi:10.1016/0378-3839(95)00036-4.

Longuet-Higgins, M. S., and R. W. Stewart (1964), Radiation stresses in water waves; a physical discussion, with applications, *Deep Sea Res. Oceanogr. Abstr.*, *11*(4), 529 – 562, doi:10.1016/0011-7471(64)90001-4.

Longuet-Higgins, M. S., and J. S. Turner (1974), An 'entraining plume' model of a spilling breaker, *J. Fluid Mech.*, *63*(1), 1 – 20, doi:10.1017/S002211207400098X.

Lubin, P., and H. Chanson (2017), Are breaking waves, bores, surges and jumps the same flow?, *Environmental Fluid Mechanics*, *17*(1), 47 – 77, doi:10.1007/s10652-016-9475-y.

Madsen, P. A., and H. A. Schäffer (1998), Higher–order boussinesq–type equations for surface gravity waves: derivation and analysis, *Philosophical Transactions of the Royal Society A*, *356*(1749), 3123 – 3181, doi:10.1098/rsta.1998.0309.

Martins, K., C. E. Blenkinsopp, and J. Zang (2016), Monitoring individual wave characteristics in the inner surf with a 2-dimensional laser scanner (LiDAR), *J. Sens., 2016*, pp. 1 – 11, doi:10.1155/2016/7965431.

Martins, K., C. E. Blenkinsopp, H. E. Power, B. Bruder, J. A. Puleo, and E. W. Bergsma (2017a), High-resolution monitoring of wave transformation in the surf zone using a LiDAR scanner array, *Coastal Eng.*, *128*, 37 – 43, doi:10.1016/j.coastaleng.2017.07.007.

Martins, K., C. E. Blenkinsopp, E. W. J. Bergsma, H. E. Power, B. Bruder, and J. A. Puleo (2017b), Remote-sensing of wave transformation in the surf zone, in *Proceedings of the Conference on Coastal Dynamics, Helsingør, Denmark*.

Martins, K., C. E. Blenkinsopp, R. Almar, and J. Zang (2017c), The influence of swash-based reflection on surf zone hydrodynamics: a wave-by-wave approach, *Coastal Eng.*, *122*, 27 – 43, doi:10.1016/j.coastaleng.2017.01.006.

Melville, W. K. (1994), Energy dissipation by breaking waves, *J. Phys. Oceanogr.*, *24*(10), 2041 – 2049, doi:10.1175/1520-0485(1994)024<2041:EDBBW>2.0.CO;2.

Michallet, H., R. Cienfuegos, E. Barthélemy, and F. Grasso (2011), Kinematics of waves propagating and breaking on a barred beach, *Eur. J. Mech. B*, *30*(6), 624 – 634, doi: 10.1016/j.euromechflu.2010.12.004.

Nairn, R., J. A. Roelvink, and H. Southgate (1990), Transition zone width and implications for modeling surfzone hydrodynamics, in *Proceedings of the 22nd Conference on Coastal Engineering, Delft, The Netherlands*, pp. 68 – 81.

Okayasu, A., T. Shibayama, and N. Mimura (1986), Velocity field under plunging waves, in *Proceedings of the 20th Conference on Coastal Engineering, Taipei, Taiwan*, pp. 660 – 674.

Peregrine, D. H. (1983), Breaking waves on beaches, *Ann. Rev. Fluid Mech.*, *15*(1), 149–178, doi:10.1146/annurev.fl.15.010183.001053.

Peregrine, D. H., and O. Bokhove (1998), Vorticity and surf zone currents, in *Proceedings of the 26th Conference on Coastal Engineering, Copenhagen, Denmark*, pp. 745 – 748.

Radon, J. (1917), Über die Bestimmung von Funktionen durch ihre Integralwerte längs gewisser Mannigfaltigkeiten, *Akad. Wiss.*, *69*, 262 – 277.

Rapp, R. J., and W. K. Melville (1990), Laboratory measurements of deep-water breaking waves, *Philosophical Transactions of the Royal Society A*, *331*(1622), 735 – 800, doi: 10.1098/rsta.1990.0098.

Rattanapitikon, W., and T. Shibayama (2000), Simple model for undertow profile, *Coastal Eng. J.*, *42*(01), 1–30, doi:10.1142/S057856340000002X.

Raubenheimer, B. (2002), Observations and predictions of fluid velocities in the surf and swash zones, *J. Geophys. Res. Oceans*, *107*(C11), 11–1 – 11–7, doi: 10.1029/2001JC001264.

Reniers, A. J. H. M., and J. A. Battjes (1997), A laboratory study of longshore currents over barred and non-barred beaches, *Coastal Eng.*, *30*(1), 1 – 21, doi:10.1016/S0378-3839(96)00033-6.

Rojas, G., and M. R. Loewen (2010), Void fraction measurements beneath plunging and spilling breaking waves, *J. Geophys. Res. Oceans*, *115*(C8).

Romero, L., W. K. Melville, and J. M. Kleiss (2012), Spectral energy dissipation due to surface wave breaking, *J. Phys. Oceanogr.*, *42*(9), 1421–1444, doi:10.1175/JPO-D-11-072.1.

Ruessink, B. G., J. R. Miles, F. Feddersen, R. T. Guza, and S. Elgar (2001), Modeling the alongshore current on barred beaches, *J. Geophys. Res. Oceans*, *106*(C10), 22,451 – 22,463, doi:10.1029/2000JC000766.

Salmon, J. E., L. H. Holthuijsen, M. Zijlema, G. P. van Vledder, and J. D. Pietrzak (2015), Scaling depth-induced wave-breaking in two-dimensional spectral wave models, *Ocean Model.*, *87*, 30 – 47, doi:10.1016/j.ocemod.2014.12.011.

Schäffer, H. A., P. A. Madsen, and R. Deigaard (1993), A Boussinesq model for waves breaking in shallow water, *Coastal Eng.*, *20*(3 – 4), 185 – 202, doi:10.1016/0378-3839(93)90001-O.

Stive, M. J. F. (1984), Energy dissipation in waves breaking on gentle slopes, *Coastal Eng.*, *8*(2), 99 – 127, doi:10.1016/0378-3839(84)90007-3.

Stive, M. J. F., and H. J. de Vriend (1994), Shear stresses and mean flow in shoaling and breaking waves, in *Proceedings of the 24th Conference on Coastal Engineering, Kobe, Japan*, pp. 594,– 608.

Stive, M. J. F., and H. G. Wind (1986), Cross-shore mean flow in the surf zone, *Coastal Eng.*, *10*(4), 325 – 340, doi:10.1016/0378-3839(86)90019-0.

Suhayda, J. N., and N. R. Pettigrew (1977), Observations of wave height and wave celerity in the surf zone, *J. Geophys. Res.*, *82*(9), 1419 – 1424, doi:10.1029/JC082i009p01419.

Svendsen, I. A. (1983), Wave heights and set-up in a surf zone, in *Hydraulic Engineering Reports*, University of Delaware.

Svendsen, I. A. (1984), Wave heights and set-up in a surf zone, *Coastal Eng.*, *8*(4), 303 – 329, doi:10.1016/0378-3839(84)90028-0.

Svendsen, I. A. (2006), *Introduction to Nearshore Hydrodynamics*, Advanced series on ocean engineering, World Scientific.

Svendsen, I. A., P. A. Madsen, and J. Buhr Hansen (1978), Wave characteristics in the surf zone, in *Proceedings of the 16th Conference on Coastal Engineering, Hamburg, Germany*, pp. 520 – 539.

Svendsen, I. A., W. Qin, and B. A. Ebersole (2003), Modelling waves and currents at the lstf and other laboratory facilities, *Coastal Eng.*, *50*(1), 19 – 45, doi:10.1016/S0378-3839(03)00077-2.

Tajima, Y. (1996), Surf zone hydrodynamics, Master's thesis, Massachusetts Institute of Technology.

Teixeira, M. A. C., and S. E. Belcher (2002), On the distortion of turbulence by a progressive surface wave, *J. Fluid Mech.*, *458*, 229 – 267, doi:10.1017/S0022112002007838.

Thornton, E. B., and R. T. Guza (1982), Energy saturation and phase speeds measured on a natural beach, *J. Geophys. Res.*, *87*(C12), 9499 – 9508.

Thornton, E. B., and R. T. Guza (1983), Transformation of wave height distribution, *J. Geophys. Res. Oceans*, *88*(C10), 5925 – 5938, doi:10.1029/JC088iC10p05925.

Tissier, M., P. Bonneton, R. Almar, B. Castelle, N. Bonneton, and A. Nahon (2011), Field measurements and non-linear prediction of wave celerity in the surf zone, *Eur. J. Mech. B*, *30*(6), 635 – 641, doi:10.1016/j.euromechflu.2010.11.003.

Tissier, M., P. Bonneton, F. Marche, F. Chazel, and D. Lannes (2012), A new approach to handle wave breaking in fully non-linear boussinesq models, *Coastal Eng.*, *67*, 54 – 66, doi:10.1016/j.coastaleng.2012.04.004.

Tissier, M., P. Bonneton, H. Michallet, and B. G. Ruessink (2015), Infragravity-wave modulation of short-wave celerity in the surf zone, *J. Geophys. Res. Oceans*, *120*(10), 6799 – 6814, doi:10.1002/2015JC010708.

Vink, A. S. (2001), Transformation of wave spectra across the surf zone, Master's thesis, Technical University of Delft.

924 Walstra, D. J. R., G. P. Mocke, and F. Smit (1996), Roller contribution as inferred from
925 inverse modelling techniques, in *Proceedings of the 25th Conference on Coastal Engi-*
926 *neering, Orlando, Florida*, pp. 1205 – 1218.
927 Yoo, J., H. M. Fritz, K. A. Haas, P. A. Work, and C. F. Barnes (2011), Depth inversion
928 in the surf zone with inclusion of wave nonlinearity using video-derived celerity, *J.*
929 *Waterway, Port, Coastal, Ocean Eng.*, *137*(2), 95 – 106, doi:10.1061/(ASCE)WW.1943-
930 5460.0000068.
931 Zelt, J. A. (1991), The run-up of nonbreaking and breaking solitary waves, *Coastal Eng.*,
932 *15*(3), 205 – 246, doi:10.1016/0378-3839(91)90003-Y.
933 Zhang, C., Y. Chen, J. Zheng, and Z. Demirbilek (2014), Variation of wave roller slope
934 in the surf zone, in *Proceedings of the 34th Conference on Coastal Engineering, Seoul,*
935 *Korea*, doi:10.9753/icce.v34.waves.12.
936 Zijlema, M., and G. Stelling (2008), Efficient computation of surf zone waves using the
937 nonlinear shallow water equations with non-hydrostatic pressure, *Coastal Eng.*, *55*(10),
938 780 – 790, doi:10.1016/j.coastaleng.2008.02.020.

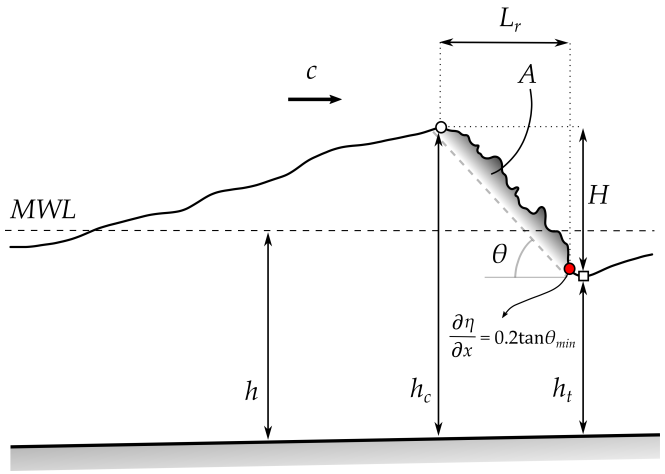

Figure 1. Definition sketch of the broken wave geometry. The mean water depth h is defined as the vertical distance between the bed and Mean Water Level (MWL). The bore propagates at speed c in water depth h_t and has a height H, corresponding to the distance between the crest (white dot) and the preceding trough (white square). The instantaneous water depth below the bore crest is expressed as $h_c = H + h_t$. The surface roller is defined from the wave crest (white dot) to the bore toe (red dot), defined as the point where $\frac{\partial \eta}{\partial x} = 0.2 \tan \theta_{max}$, where θ_{max} is the maximum angle found over the roller region. The surface roller has an angle with the horizontal of θ and a length L_r. Finally, the surface roller area is noted A but is only represented schematically here, due to the lack of definition and knowledge on this quantity and on ρ_r.

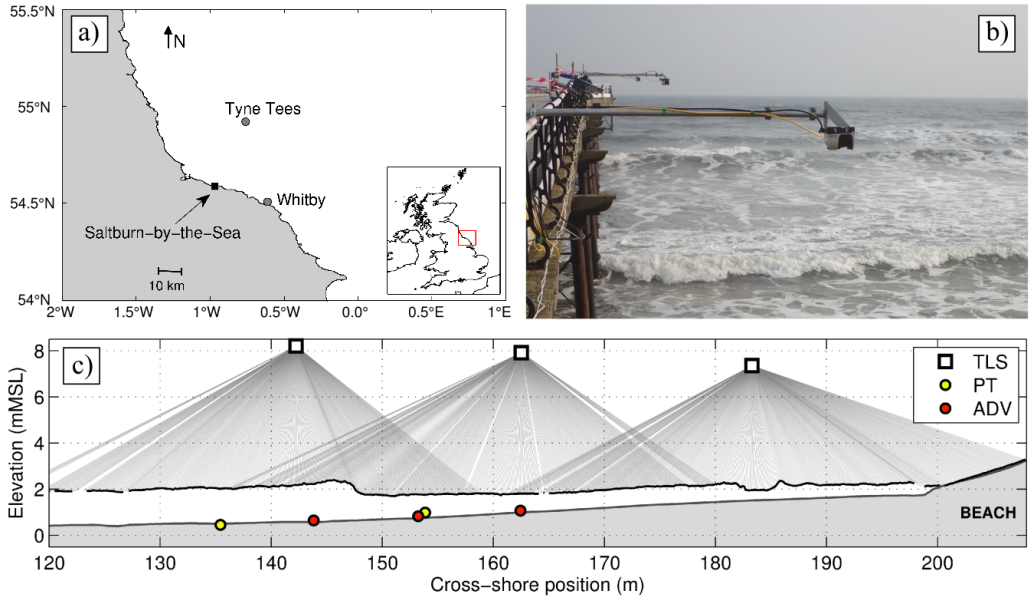

Figure 2. Field site and LiDAR scanner deployment. The regional map around Saltburn-by-the-Sea, UK, is shown in panel a). The location of the nearshore (Whitby) and offshore (Tyne Tees) wave buoys are shown by the grey dots. Panel b) shows the LiDAR scanner deployment on the nearshore pier: the scanners were deployed 2.5 m away from the pier, using a 'T' shaped scaffolding system fixed to the pier railing. Panel c) shows a schematic of the experimental set-up with an example of post-processed free surface elevation (black thick line while individual measurements are shown as light grey lines). The beach profile (thick grey line) corresponds to the surveyed profile during the previous low tide (10/04/16).

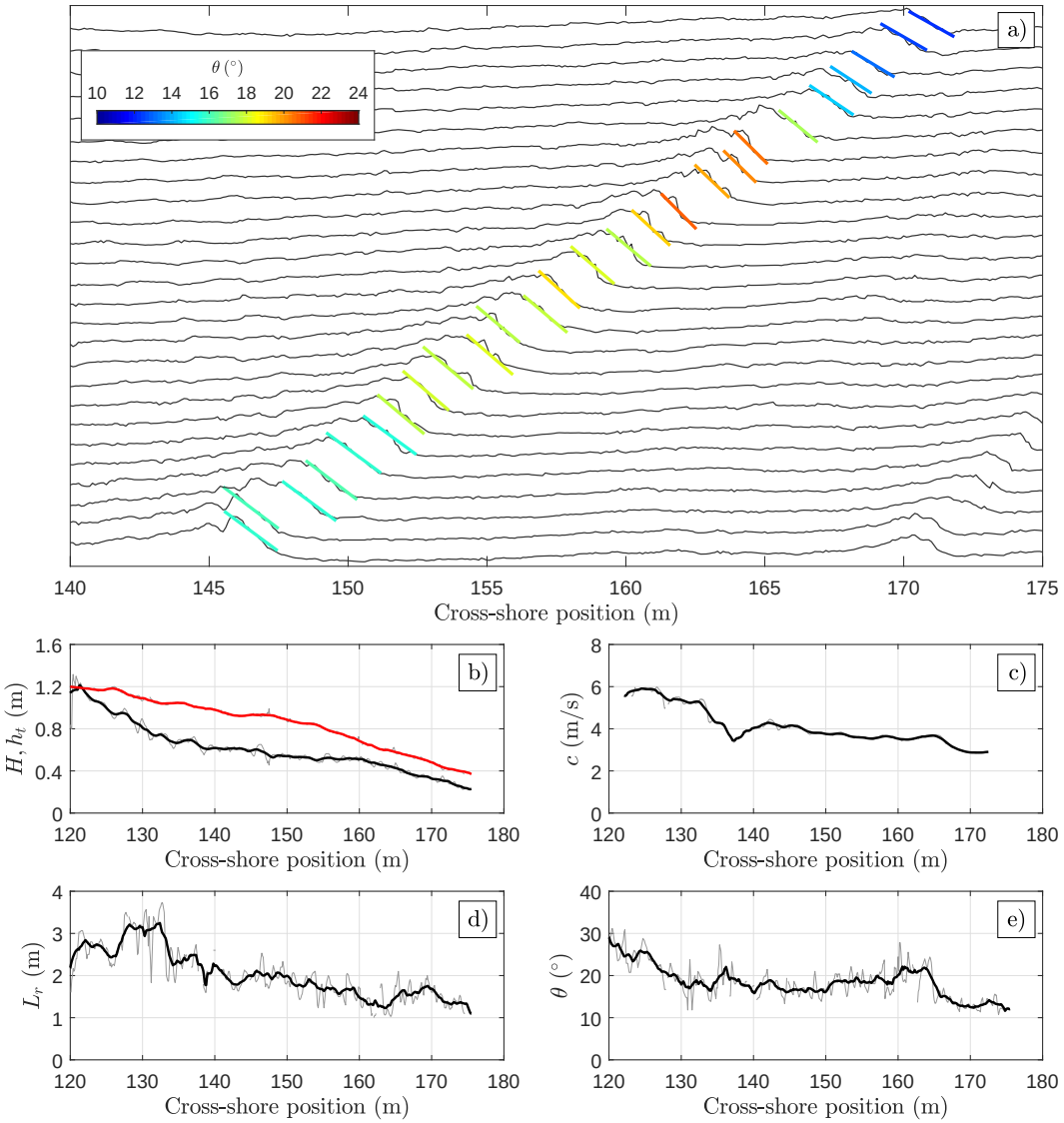

Figure 3. Example of a tracked bore in the inner surf zone on 09/04. Panel a) shows the wave profile changes every metre along a section (between $x = 145$ and 170 m) of the full wave track. The linear fit of the roller surface measurements is added at every location, coloured by the roller angle. Panels b-e) show the cross-shore evolution of the individual wave height H (black line) and local water depth h_t (red line), celerity c, the roller length L_r and angle θ respectively. The raw measurement is shown as a thin grey line, while the moving window-averaged ($\Delta x = 2$ m) signal is shown as black thick line (red for h_t).

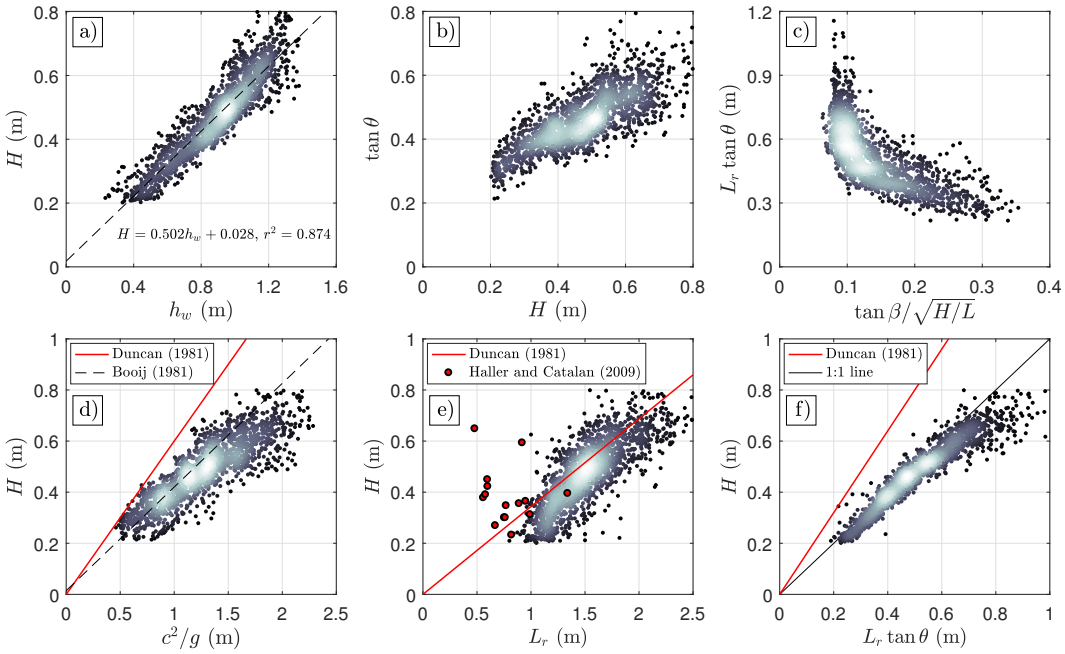

Figure 4. Individual wave properties of the 38 inner surf zone waves constituting the present dataset. In each panel, data are shown as a scatter plot coloured by the cloud point density: the brighter region is the densest area whereas darker dots show sparser data points. Panel a) first shows the individual wave height H against the period-averaged water depth h_w. Panel b) shows the surface roller front slope $\tan\theta$ as a function of H. Panel c) shows the quantity $L_r \tan\theta$ as a function of the local Iribarren number ($\tan\beta$ is the local beach slope and L a wave length estimated as cT). Panels d-f) show the comparison of c^2/g, L_r and $L_r \tan\theta$ against H and the relations from *Duncan* [1981].

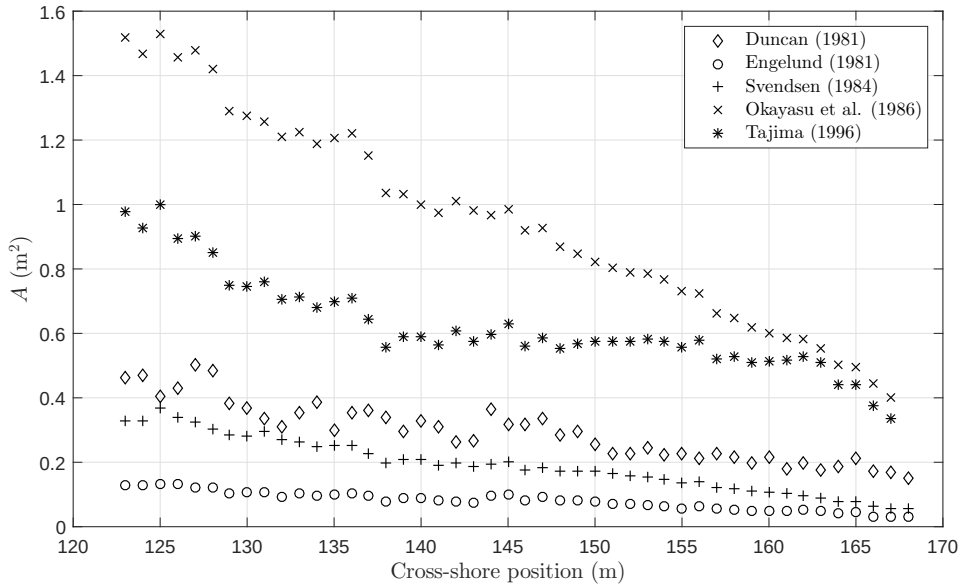

Figure 5. Cross-shore evolution of the surface roller area computed from the formulations presented in Table 1 using the ensemble-averaged properties of a wave group from 09/04/2016 (composed of 6 consecutive and similar waves, see Appendix).

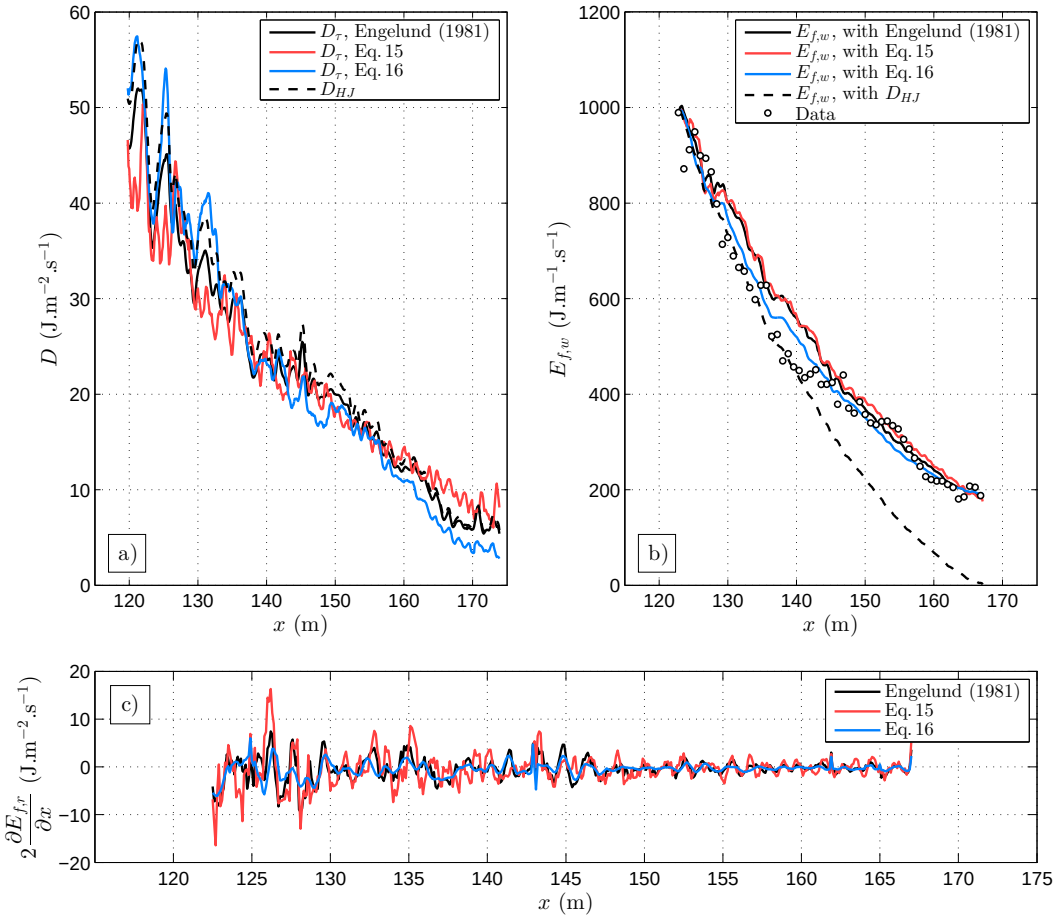

970 **Figure 6.** Results from the roller model against the wave group ensemble-averaged data, using $\rho_r = 0.87\rho$
971 (same wave group as Figure 5, see also Appendix). Panel a) shows the dissipations terms D_τ computed using
972 the roller area formulations from *Engelund* [1981] and the modified formulations of D81 (Eq. 15) and S84
973 (Eq. 16). The dissipation term D_{HJ} (Eq. 13) of a hydraulic jump of the same height is also shown. Panel b)
974 shows the cross-shore evolution of the modelled incident wave energy flux (Eq. 7) computed with the dissipa-
975 tion terms from panel a). The spatial variation of the roller kinetic energy computed with a factor 2 is shown
976 in panel c) for the three roller area formulations.

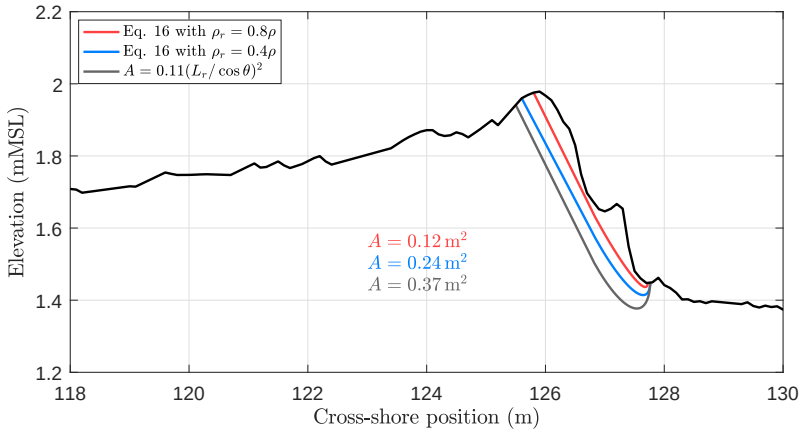

977 **Figure 7.** Surface roller areas shown under an example wave profile (4th wave of the group, see Appendix).
978 To facilitate the calculation of the roller area, the interface between the roller and the wave was assumed to
979 have an ellipsoidal shape close to the roller toe.

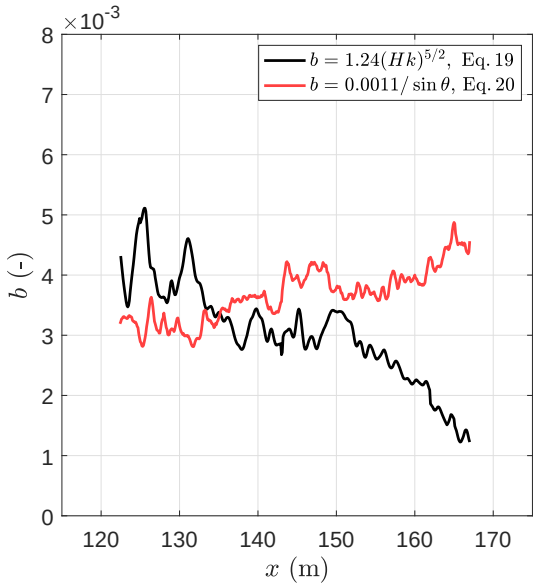

Figure 8. Cross-shore evolution of the dissipation coefficient b (Eq. 17), computed with the wave group ensemble-averaged data (same wave group as Figure 5) using the formulation of D81 (Eq. 20) and that found later by *Drazen et al.* [2008] (Eq. 19).

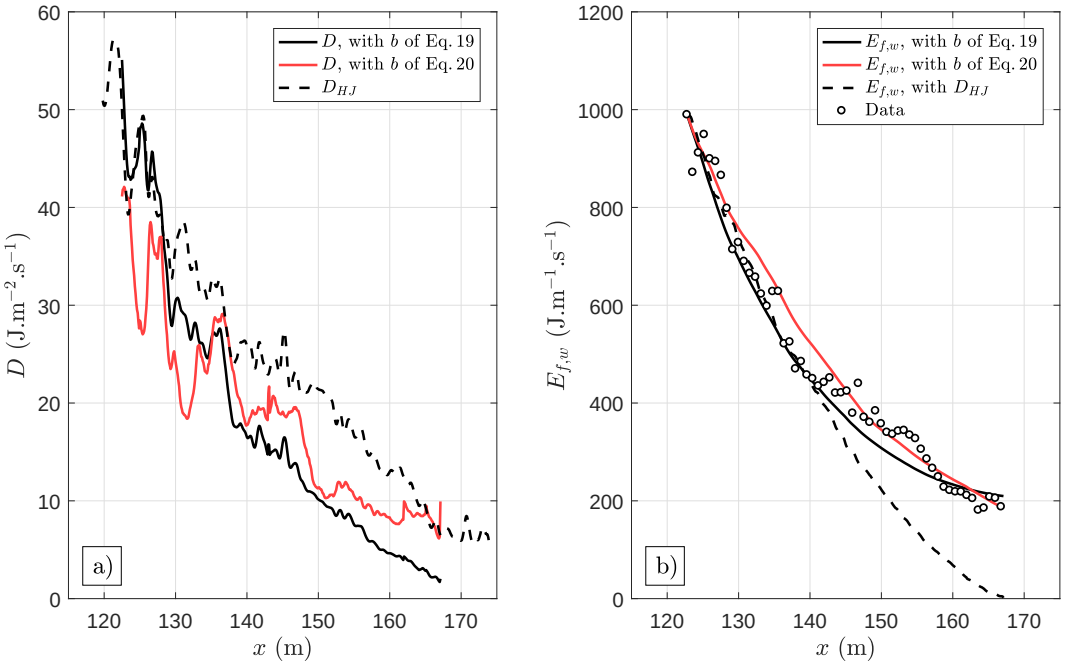

Figure 9. Results from the energy balance model of Eq. 16 against the wave group ensemble-averaged data (same wave group as Figure 5, 6 and 8, see also Appendix). Panel a) shows the dissipations terms D computed using the two formulations for b (Eq. 19 and 20). The dissipation term D_{HJ} of a hydraulic jump of the same height is also shown as indication. Panel b) shows the cross-shore evolution of the modelled incident wave energy computed with the dissipation terms from panel a).

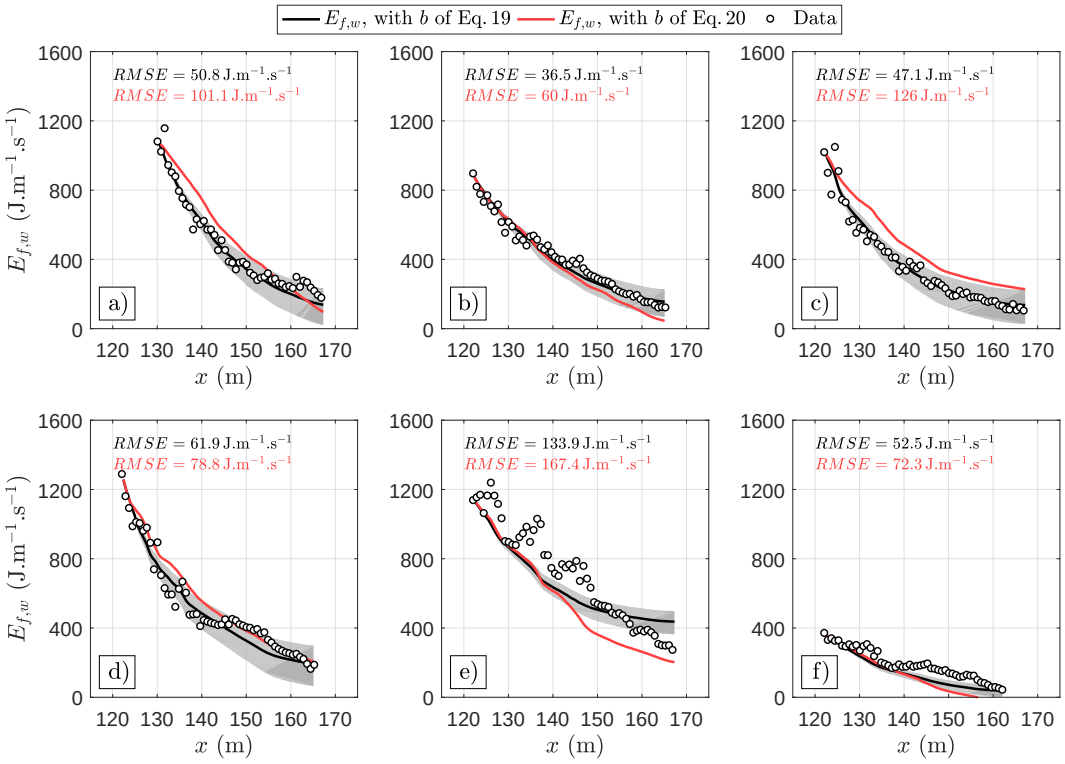

988 **Figure 10.** Results from the energy balance model of Eq. 16 at the wave-by-wave scale against measure-
989 ments from the same wave group as Figures 5, 6, 8 and 9. If we number the individual waves by order of
990 apparition (see Figure A.1), panels a, b, c, d, e and f show the modelled wave energy flux for the waves num-
991 ber 1, 2, 3, 4, 5 and 6 respectively. To highlight the sensitivity of the model to the individual wave period, the
992 results for Eq. 19 and obtained with $T \pm 1$ s are indicated by the gray region.

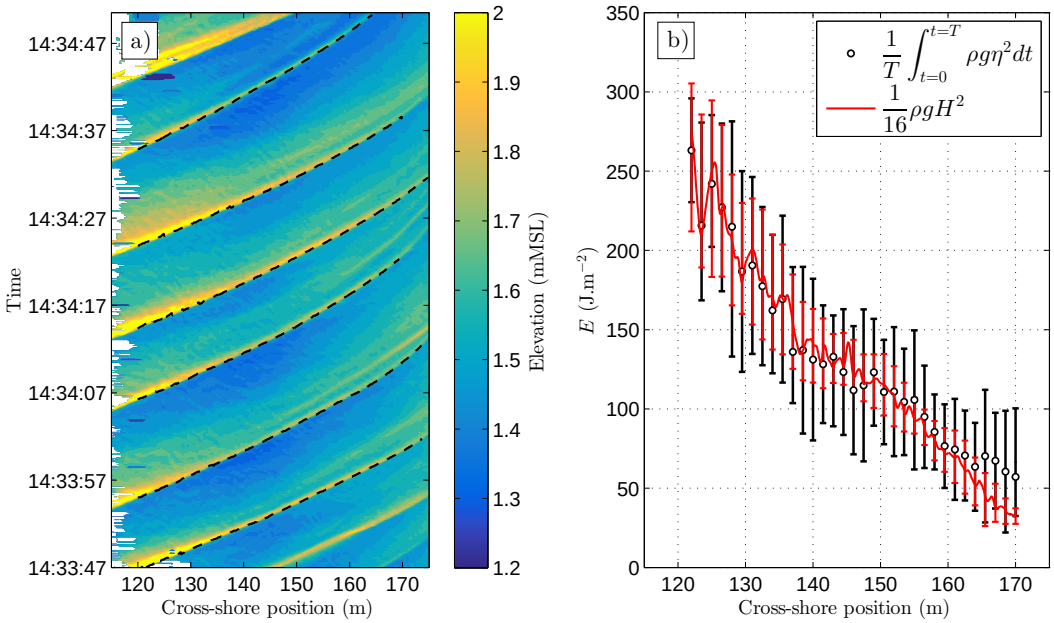

Figure A.1. Presentation of the wave group selected for the analysis. Panel a) shows the surface elevation timestack in the Mean Sea Level (MSL) referential. The wave crest tracks are shown as black dashed lines. Panel b) compares the ensemble-averaged wave energy computed with the integral form (Eq. 7) and linear wave theory with $B_0 = 0.0625$ (Eq. A.1). For both energy formulation, the standard deviation is shown as error bar in the same colour.

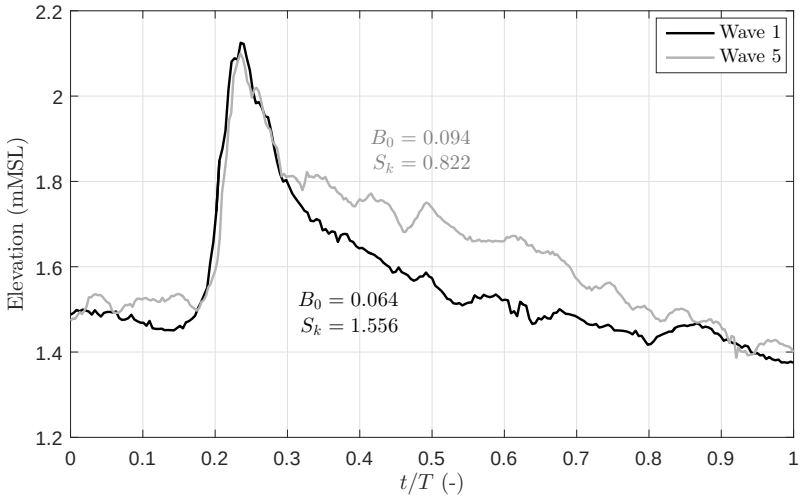

998 **Figure A.2.** Temporal wave profile at $x = 130$ m of the individual wave number 1 and 5 of the wave group
999 from Figure A.1a.